Processes and time scales of dacite magma assembly and eruption at Tauhara volcano, Taupo Volcanic Zone, New Zealand

Marc-Alban Millet

School of Geography, Environment and Earth Sciences, Victoria University of Wellington, Wellington, New Zealand

Origins Laboratory, Department of the Geophysical Sciences, University of Chicago, Chicago, Illinois, USA

Now at Department of Earth Sciences, Durham University, South Road, Durham DH1 3LE, UK (m.a.millet@durham.ac.uk)

Chelsea M. Tutt and Monica R. Handler

School of Geography, Environment and Earth Sciences, Victoria University of Wellington, Wellington, New Zealand

Joel A. Baker

School of Geography, Environment and Earth Sciences, Victoria University of Wellington, Wellington, New Zealand

Now at School of Environment, University of Auckland, Auckland, New Zealand

[1] Magma mixing plays a prominent role in the origins of intermediate magmas in subduction zones. However, the conditions and time scales of magma mixing and how these are linked to subsequent eruption are unclear. Mount Tauhara is the largest dacitic volcanic complex in the Taupo Volcanic Zone, New Zealand. Dacites from Tauhara volcano have a complex petrography (Qtz + Plag + Amph + OPx + CPx + Oxi ± Oli) that can only have been produced by magma mixing and offer an ideal opportunity to investigate the processes and time scales involved in assembling dacite magmas in a continental subduction zone. Here, we present whole-rock and mineral-specific major and trace element and isotopic data for the Tauhara dacites in order to identify the magma mixing end-members, constrain the physical conditions of mixing, and estimate the time scales and relationships between magma mixing, ascent, and eruption. These data reveal that four separate mixing events between crystal-rich rhyolites (77–80 wt % SiO_2; 40 ppm Sr) and crystal-poor mafic magmas of basaltic (48 wt % SiO_2; 1340 ppm Sr) to andesitic (55–59 wt % SiO_2; 490–580 ppm Sr) composition occurred to produce the Tauhara dacites. Mixing took place in well-stirred magma chambers located at midcrustal depths (8–13 km) at temperatures from 840 to 900°C. The time scales of magma mixing obtained from Ti diffusion in quartz appear to be largely dependent on the temperature and viscosity contrast between the end-members as andesite and rhyolite magma mixed on time scales of 2–7 months, whereas basalt and rhyolite magmas mixed on time scales of 1–2 years. The short magma mixing time scales, combined with the physical properties (e.g., viscosity and density) of the mixed dacite magmas, as compared with those of the end-member magmas, facilitated the ascent and eruption of dacite magmas at Tauhara volcano.

Components: 14,646 words, 16 figures, 3 tables.

1. Introduction

[2] The processes and time scales leading to the genesis of intermediate magmas such as andesite and dacite in continental settings is a fundamental question in Earth Sciences. Magmas with intermediate compositions are widely erupted at convergent plate tectonic margins, particularly in continental settings [*Rudnick*, 1995]. However, it is unclear whether most of these rocks are solely the product of magma differentiation or are, in fact, hybrid products of mixing silicic magmas with a crystal cargo that biases the whole-rock chemistry to an intermediate composition [*Reuby and Blundy*, 2009]. The continental crust has a bulk composition that resembles intermediate magmas produced at subduction zones [*Rudnick and Fountain*, 1995], and the origins of such rocks are also central to our understanding of the formation and evolution of continental crust [*Reuby and Blundy*, 2009; *Rudnick*, 1995]. Moreover, understanding the mechanisms by which intermediate magmas form, and the time scales for their assembly, ascent and eruption, is important as these magmas form volcanoes that represent major volcanic hazards in some of the most volcanically active regions on Earth.

[3] A variety of magmatic processes have been invoked to account for the formation of andesitic and dacitic magmas. Whilst not mutually exclusive, three main mechanisms have been proposed, including partial melting of hybridized mantle wedge or crustal material [*Carmichael*, 2002; *Hirose*, 1997; *Turner et al.*, 2000], extensive fractional crystallization of mafic mantle-derived melts [*Garrison et al.*, 2012; *Pichavant et al.*, 2002] and mixing between mafic and silicic magmas and their crystal cargoes [*Eichelberger et al.*, 2006; *Kent et al.*, 2010; *Reuby and Blundy*, 2009; *Schiano et al.*, 2010]. In situ or crystal-specific chemical and isotopic investigations are a particularly powerful tool to investigate magma mixing processes and time scales [e.g., *Costa et al.*, 2010; *Morgan et al.*, 2004]. Mineral textures and chemistry, including those of crystal-hosted melt inclusions, can reveal the origins, conditions of crystallization, residence times, and ascent rates of crystals in volcanic rocks, which cannot be readily elucidated from study of whole-rock samples [e.g., *Davidson et al.*, 2007].

[4] We have used a range of crystal-specific investigations to examine the conditions and timing of assembly and eruption of dacitic magmas from Tauhara volcano in the Taupo Volcanic Zone (TVZ), New Zealand. Tauhara volcano is a ca. 190 ka [*Wilson et al.*, 1995] dacite complex located on the rim of a continental back-arc rift (TVZ), associated with active subduction of the Pacific Plate beneath the Australian Plate in northern New Zealand. A previous study by *Graham and Worthington* [1988] used petrographic, and whole-rock chemical and isotopic evidence to show that the dacites of Tauhara volcano were the products of magma mixing between at least three different melts.

[5] Tauhara volcano lavas have a complex petrographic assemblage, including olivine, plagioclase, clinopyroxene, orthopyroxene, amphibole, Fe-Ti oxide, and quartz phenocrysts. In addition to whole-rock major and trace element, and Pb-Sr isotope data, we present a detailed chemical and isotopic study of most of these mineral phases, as well as quartz-hosted melt inclusions. The crystal-specific data make it possible to gain novel insights into the mixing end-members that

produced the dacitic magmas of Tauhara volcano, fingerprint the origins of their crystal cargoes, and estimate the time scales and locations of magma mixing and subsequent eruption. Our results show that magma mixing between different mafic and silicic end-members took place at lower to mid-crustal depths of 8–13 km, and that magmatic hybridization took several months, and was followed by rapid magma ascent and ensuing eruption on time scales of weeks.

2. Geological Background

[6] The North Island of New Zealand lies on an active convergent plate boundary where the Pacific Plate is obliquely subducting beneath the Australian Plate [*Cole and Lewis*, 1981] to form the Taupo-Hikurangi arc-trench system (Figure 1). The Taupo-Hikurangi system marks the southernmost 300 km of the 2000 km long Tonga-Kermadec-Taupo volcanic arc and associated Lau-Havre-Taupo back-arc system, which is undergoing a southward propagation from rifting to spreading [*Parson and Wright*, 1996]. The TVZ is an active continental region of back-arc rifting and Cenozoic arc volcanism. The extensional regime of the TVZ began ca. 4 Ma with present-day extension and subsidence rates from 12 to 20 mm/yr and up to 3 mm/yr, respectively [*Parson and Wright*, 1996]. Subduction-related volcanism began in the TVZ at ca. 2 Ma with rhyolitic (and minor basaltic, andesitic, and dacitic) activity from ca. 1.6 Ma [*Wilson et al.*, 1995]. The TVZ can be divided into three segments: northern and southern regions dominated by basaltic andesite to dacite volcanoes and a central 125 km segment dominated by eight caldera-forming rhyolitic centers (Figure 1) [*Healy*, 1962].

[7] Dacites comprise <0.1% of the total volume of TVZ eruptives with no individual volcanic complex or flow having a volume >3 km³ [*Graham and Worthington*, 1988]. Exposed dacites in the TVZ have been divided into two geochemical groups (Type A and B) by *Graham et al*. [1995]. Type A dacites are postulated to have formed by the fractionation of a high-alumina basalt (HAB) and are commonly associated with the HAB andesite sequence with ≤67 wt % SiO_2. These andesite-dacite suites are principally located in the northern and southern regions of the TVZ. Type B dacites are typically found in the central TVZ and have 64–70 wt % SiO_2 and lower large ion lithophile element concentrations and $^{87}Sr/^{86}Sr$ ratios than Type A dacites. Type B dacites appear to be
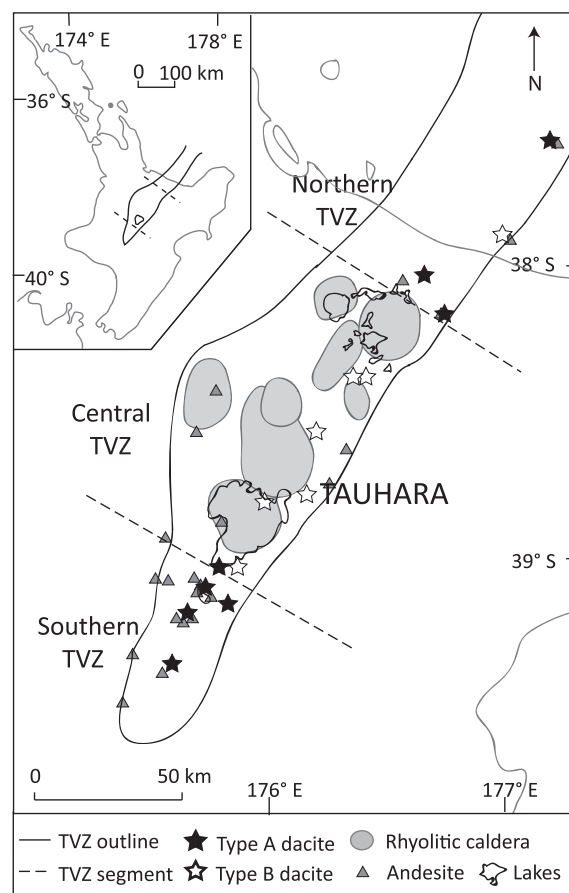

Figure 1. Map showing the areal extent of the Taupo Volcanic Zone (TVZ) and its segments as described by *Healy* [1962] and *Wilson et al*. [1995]. The locations of andesite and dacite volcanoes (labeled) and the eight calderas formed by rhyolitic pyroclastic eruptions are also shown.

genetically related to rhyolites either through fractionation-accumulation or magma mixing processes [*Graham and Worthington*, 1988].

[8] Mt Tauhara is the site of the largest known TVZ dacitic complex, and is classified as a Type B dacite [*Graham and Worthington*, 1988]. Tauhara volcano is situated 5 km northeast of Taupo city on the eastern rim of the central segment of the TVZ (Figure 1). Tauhara volcano comprises six dacite domes (Western, Central, Hipaua, Trig M, Breached, and Main), one rhyolite flow (Trig 9471), and two inferred dacite domes. The two inferred domes are a cryptodome (Buried) beneath a pyroclastic flow erupted from Breached dome, and a dome adjacent to the main edifice (Waipahihi) interpreted to be dacitic in composition from (or based on) an electrical resistivity survey [*Dawson and Thompson*, 1981] (Figure 2), but for
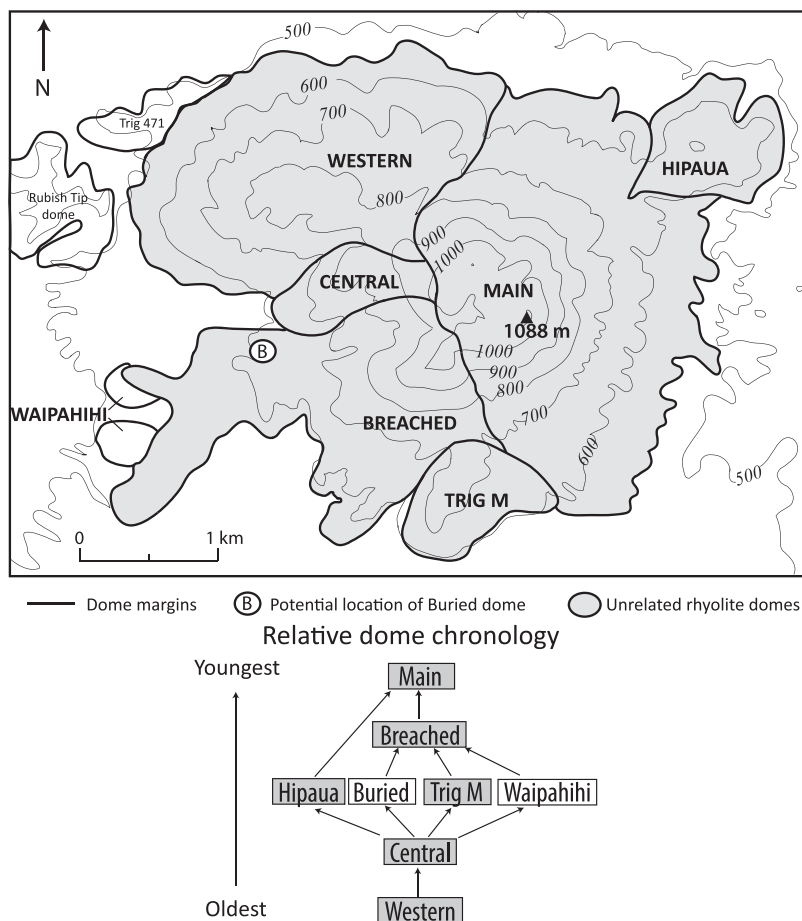
Figure 2. Map of Tauhara volcano showing the location and extent of domes, lava flows, and other features identified by *Worthington* [1985].

which no samples could be collected due to the lack of rock exposures. The rhyolite of Trig 9471 and adjacent Rubbish Tip dome are chemically unrelated to the Tauhara dacites and are more closely related to the ca. 50 ka Ngangiho dome located ca. 8 km to the northwest of Tauhara volcano [*Sutton et al.*, 1995]. The exposed volume of the Tauhara dacite complex is ca. 1 km³. However, the base of the volcano is buried by younger ignimbrites and air fall deposits (e.g., eruptives from the Taupo caldera) [*Wilson*, 1993], which makes it likely that the entire volume of Tauhara volcano is considerably larger than 1 km³. Relative dome ages have been constrained from field relationships by *Worthington* [1985], with Western dome inferred to be the oldest, followed by Central dome. Hipaua, Trig M, Buried, and Waipahihi domes form isolated domes and are only known to be older than Breached dome. Superimposed on all domes is the youngest and largest Main dome.

[9] Tauhara dacites from the different domes all have similar mineral assemblages with ca. 20%

modal phenocrysts [*Worthington*, 1985]. Plagioclase is the most abundant phenocryst (ca. 10%) and exhibits extensive disequilibrium features including sieve textures. Orthopyroxene and clinopyroxene are also present with average phenocryst contents of ca. 1% and 2%, respectively. Both clinopyroxene and orthopyroxene occur as euhedral to subhedral individual phenocrysts and monominerallic and clinopyroxene-orthopyroxene clusters with no chemical distinctions between forms. Hornblende (ca. 3%) has destabilized rims in samples form all domes apart from Main dome. Quartz is also present (1%–2%) as anhedral crystals with abundant fractures. Olivine and biotite are both present in trace amounts as subhedral to anhedral crystals.

3. Samples and Analytical Methods

[10] One hundred and fifteen samples were collected by *Worthington* [1985] from six domes;

Western, Central, Hipaua, Trig M, Breached and Main domes, and associated pyroclastic flows. We selected 33 representative samples for further investigation based on major element and modal mineralogy variations. The trace element chemistry of these samples was measured using solution inductively coupled plasma-mass spectrometry (ICP-MS). From these 33 samples, 21 samples were analyzed for Sr-Pb isotopes using multiple-collector ICP-MS. Six representative samples, one from each dome, have been subjected to detailed in situ mineral major and trace element analysis by electron probe microanalysis and laser ablation ICP-MS, respectively. Groundmass and mineral separates (clinopyroxene, plagioclase, and amphibole) from these six samples were also analyzed for Sr-Pb isotopes by MC-ICP-MS. Full details of sample descriptions, analytical methods and standard data are presented as supporting information.[1]

[11] Diffusion modeling was applied to quartz rim zones using the one-dimensional method of *Morgan et al.* [2004]. Quartz diffusion coefficients were calculated using the methods of *Cherniak et al.* [2007]. Examples of modeled phenocrysts are presented in the supporting information. Whole quartz crystals were separated from crushed rock samples and mounted in epoxy so that the *c* axes were flat.

4. Results

4.1. Major and Trace Element Data

4.1.1. Whole-Rock Samples

[12] Representative major and trace element data for the Tauhara dacites are presented in Table 1, and all analyses are available as supporting information. SiO_2 contents range from 64.6 to 71.5 wt %, with data for samples from both Western and Main domes spanning this entire range. Two samples from Central dome have SiO_2 contents of 68.5 and 71.0 wt %. Hipaua and Trig M dome samples have a smaller range of SiO_2 contents from 66.7 to 69.4 wt % and 64.6 to 66.2 wt %, respectively. Samples from the Breached dome edifice have SiO_2 contents comparable to Trig M dome samples.

[13] Data for other major elements correlate linearly with SiO_2 (e.g., Figure 3) A negative trend is

observed between SiO_2 and Al_2O_3 and FeO, whereas K_2O exhibits a positive trend with SiO_2. While different domes have overlapping SiO_2-K_2O arrays, subtly different subparallel arrays are observed for other elements such as FeO and TiO_2 versus SiO_2 (Figures 3a and 3c).

[14] Overall, transition metal and Sr, Zr, and Hf concentrations correlate negatively with SiO_2, and only Rb and Nb correlate positively with SiO_2 (Figure 3; only Sr, Rb, V, and Ni are shown). In more detail, dome-specific trends can be discerned for Sc, Cr, Ni, Cu and, in particular, Sr when plotted versus SiO_2 (e.g., Figures 3e and 3h). Samples from Western and Central domes have higher Sr, Cr, Ni, and Cu and lower Sc at a given SiO_2 content relative to samples from Breached and Main domes. Data for Hipaua and Trig M dome samples display distinct characteristics, plotting with data for Western and Central dome samples on the low Sc array, but with data for Breached and Main dome samples on the low Sr and Cu arrays. Furthermore, data for samples from Hipaua and Trig M domes plot in distinct fields (or trends) for Cr and Ni versus SiO_2.

[15] Other incompatible trace elements, including Y, Ba, rare earth elements (REE), U, Th, and Pb show little variation with SiO_2. However, REE data define two sample groupings with the Western and Central dome samples having higher light REE and lower heavy REE concentrations ($La/Yb_N = 8–11$) than the other domes ($La/Yb_N = 6–8$) (see supporting information).

4.1.2. Amphibole

[16] Amphibole major and trace element data are plotted versus Al_2O_3 in Figure 4. Two populations of amphibole are observed. High Al_2O_3 (8.5–12.5 wt %) amphiboles are found in samples from all domes. In this population, no systematic differences are found between cores and rims. A second population with distinctly lower Al_2O_3 (6.0–7.5 wt %) forms rims on some amphibole crystals from Main dome.

[17] Data for most trace elements do not show clear trends with Al_2O_3. However, amphiboles from Western and Central domes exhibit higher Sr, Ni and lower Sc at a given Al_2O_3 than amphiboles from the other domes, which mimics the differences observed in whole-rock trace element data between domes. Amphibole rims with low Al_2O_3 from Main dome have markedly different trace element concentrations when compared with the other amphiboles (e.g., low Sr, Ni, and Eu/

Table 1. Representative Whole-Rock Major and Trace Element and Sr-Pb Isotope Data for Tauhara Dacites

Dome	Western			Central		Hipaua		Trig M		Breached			Main		
Sample	421	427	437	439	442	452	456	473	478	488	497	498	521	527	528
SiO_2	65.01	67.23	71.36	68.48	66.75	67.20	69.42	64.61	66.22	68.55	64.74	65.83	64.62	71.54	67.50
TiO_2	0.43	0.39	0.33	0.37	0.39	0.38	0.34	0.45	0.44	0.41	0.49	0.46	0.50	0.32	0.41
Al_2O_3	16.09	14.84	14.61	14.94	14.91	14.83	14.53	15.72	15.65	14.33	15.44	15.31	15.26	14.09	14.81
Fe_2O_3 tot	4.72	4.07	3.09	3.78	4.47	4.28	3.65	5.25	4.84	4.59	5.11	4.90	5.26	3.09	4.37
MnO	0.05	0.07	0.06	0.07	0.08	0.10	0.06	0.14	0.07	0.09	0.10	0.10	0.10	0.07	0.08
MgO	2.91	2.63	1.13	2.07	2.63	2.57	1.92	3.01	2.56	2.11	3.04	2.75	3.20	1.29	2.41
CaO	5.21	4.98	3.21	4.72	4.80	4.65	3.78	5.56	4.72	3.85	5.61	5.08	5.71	3.14	4.60
Na_2O	3.56	3.45	3.72	3.46	3.68	3.73	3.84	3.46	3.38	3.70	3.42	3.38	3.30	3.76	3.55
K_2O	1.94	2.23	2.47	2.03	2.20	2.18	2.39	1.70	2.05	2.29	1.94	2.08	1.93	2.66	2.18
P_2O_5	0.08	0.11	0.02	0.08	0.09	0.08	0.07	0.10	0.07	0.08	0.11	0.11	0.12	0.04	0.09
LOI	2.41	0.29	0.80	1.14	1.02	0.11	0.12	0.73	0.77	0.92	0.98	1.49	0.91	2.30	0.95
Total	100.03	99.74	99.80	99.62	99.61	100.26	100.45	99.77	99.60	99.50	100.16	99.66	99.93	99.74	99.91
Sc	13.3	11.2	8.46	8.96	11.4	11.3	9.24	12.9	11.8	13.0	15.0	13.9	15.8	8.08	12.8
V	97.8	54.8	43.9	65.4	84.7	82.0	61.7	108	96.7	80.8	113	94.3	114.9	44.3	85.0
Cr	72.0	57.5	18.3	35.5	45.7	44.9	31.3	36.0	29.1	36.4	45.5	38.0	48.4	17.4	38.6
Ni	50.5	42.3	14.4	22.8	33.3	34.2	24.5	30.8	33.7	18.1	22.6	19.1	23.6	8.42	17.6
Cu	56.8	47.6	26.9	26.9	18.9	20.6	16.6	19.1	24.3	12.5	22.7	21.8	14.2	12.1	15.2
Zn	46.2	49.6	40.9	45.5	52.8	51.4	44.5	62.1	56.2	57.3	57.8	57.6	60.2	39.6	53.6
Ga	17.3	n.d	16.0	n.d	15.9	16.2	15.2	16.9	16.3	16.4	16.4	n.d	15.5	n.d	15.6
Rb	52.2	57.0	74.3	58.9	65.7	63.8	73.4	43.1	56.0	69.2	55.7	60.1	53.1	70.7	68.6
Sr	658	549	461	538	330	331	267	389	345	311	361	321	342	185	292
Y	12.1	16.1	14.9	13.8	16.6	17.3	17.1	15.8	14.0	14.9	18.7	18.2	17.6	17.0	19.9
Zr	112	83.3	80.2	92.9	100.3	97.5	56.4	85.4	79.3	85.3	114	106	104	68.4	97.0
Nb	5.19	5.03	6.01	4.64	4.92	4.98	5.12	4.41	4.52	5.65	5.33	5.45	4.98	5.14	5.55
Mo	0.868	0.398	0.657	0.792	0.879	0.895	0.922	0.769	1.22	1.13	0.832	0.935	0.871	1.00	0.935
Cs	2.42	1.87	1.76	2.62	2.93	1.88	2.28	2.10	1.99	2.60	2.53	2.68	2.42	3.09	3.06
Ba	617	533	608	460	483	501	519	433	487	532	467	470	420	465	527
La	18.9	22.4	25.5	16.9	17.1	17.7	18.8	16.0	14.6	21.0	18.0	16.9	16.4	16.1	19.2
Ce	35.2	43.9	48.2	33.2	34.2	35.1	36.8	31.9	28.0	41.2	36.6	35.4	33.4	32.5	39.0
Pr	3.95	5.04	5.35	3.73	3.89	4.04	4.35	3.77	3.20	4.43	4.35	4.01	3.94	3.66	4.50
Nd	14.4	18.6	18.1	13.7	14.5	15.2	16.0	14.5	12.0	14.7	16.7	15.3	15.2	13.5	17.0
Sm	2.80	3.53	3.09	2.59	2.93	3.15	3.24	3.03	2.56	2.65	3.41	3.11	3.08	2.70	3.44
Eu	1.00	0.867	0.837	0.697	0.784	0.797	0.745	0.809	0.768	0.828	0.918	0.814	0.810	0.659	0.899
Gd	2.80	3.36	3.29	2.60	3.08	3.16	3.18	3.04	2.52	2.76	3.50	3.18	3.10	2.80	3.58
Tb	0.401	0.468	0.467	0.377	0.465	0.484	0.493	0.460	0.397	0.411	0.524	0.484	0.477	0.430	0.543
Dy	2.33	2.70	2.70	2.24	2.79	2.91	2.95	2.72	2.44	2.60	3.17	2.93	2.90	2.60	3.30
Ho	0.463	0.536	0.543	0.452	0.572	0.590	0.595	0.561	0.491	0.542	0.652	0.608	0.591	0.541	0.696
Er	1.38	1.62	1.61	1.38	1.75	1.80	1.76	1.66	1.49	1.68	1.96	1.83	1.74	1.64	2.10
Tm	0.207	0.240	0.233	0.209	0.261	0.272	0.259	0.246	0.221	0.258	0.287	0.275	0.255	0.248	0.318
Yb	1.43	1.58	1.60	1.40	1.77	1.86	1.72	1.67	1.54	1.76	1.92	1.83	1.76	1.68	2.13
Lu	0.216	0.242	0.240	0.221	0.271	0.290	0.256	0.256	0.237	0.274	0.309	0.288	0.274	0.261	0.336
Hf	3.42	2.61	2.57	2.67	2.81	2.93	1.91	2.57	2.44	2.61	3.14	2.84	2.71	2.04	2.89
Ta	0.701	0.483	0.626	0.468	0.466	0.486	0.508	0.561	0.488	0.867	0.504	0.505	0.477	0.530	0.599
Pb	11.3	8.53	11.8	11.1	11.6	11.2	10.5	9.76	12.4	18.1	11.6	10.2	7.6	10.8	14.3
Th	8.91	7.80	8.76	7.04	7.61	7.91	7.14	6.79	6.85	7.95	7.12	6.91	6.10	7.11	8.25

Table 1. (continued)

Sample Dome	Western			Central	Hipaua			Trig M		Breached			Main		
	421	427	437	439	442	452	456	473	478	488	497	498	521	527	528
U	2.13	1.42	1.75	1.52	1.75	1.79	1.59	1.55	1.60	1.66	1.66	1.62	1.49	1.64	1.90
$^{206}Pb/^{204}Pb$	18.801	18.811	18.832	18.811			18.828	18.812	18.811		18.797	18.799	18.797	18.829	18.810
2sig	0.001	0.001	0.001	0.001			0.001	0.001	0.001		0.001	0.001	0.001	0.002	0.001
$^{207}Pb/^{204}Pb$	15.614	15.619	15.627	15.621			15.630	15.624	15.617		15.618	15.613	15.618	15.629	15.617
2sig	0.001	0.001	0.001	0.001			0.001	0.001	0.001		0.001	0.001	0.001	0.002	0.001
$^{208}Pb/^{204}Pb$	38.676	38.695	38.724	38.706			38.731	38.717	38.691		38.688	38.675	38.690	38.724	38.686
2sig	0.003	0.003	0.004	0.002			0.002	0.003	0.003		0.003	0.004	0.002	0.005	0.003
$^{87}Sr/^{86}Sr$	0.704402	0.704245	0.704322	0.704513			0.704764	0.704758	0.704802		0.704842	0.704853	0.704866	0.704293	0.704677
2sig	0.000012	0.000006	0.000011	0.000008			0.000007	0.000007	0.000007		0.000013	0.000013	0.000009	0.000011	0.000010

Eu*; high REE), but extend the overall trace element trends observed for the other amphiboles.

4.1.3. Clinopyroxene

[18] Most clinopyroxenes have major element compositions of $Wo_{40–50}En_{40–50}Fs_{20–10}$ with no clear systematic variation between domes (see supporting information). The Mg number (Mg#) of clinopyroxene is plotted versus concentration data for selected trace elements in Figure 5. Two populations of clinopyroxene can be identified on the basis of Mg#. Most clinopyroxenes have Mg# = 70–85 with a smaller, more mafic, population with Mg# = 85–90, which comprises clinopyroxene from Western, Central, and Hipaua domes. Similarly to the main population of amphiboles, no systematic differences between cores and rims have been found in the chemistry of the main clinopyroxene population. However, the second population (with higher Mg#) only corresponds to cores or middle zones of measured clinopyroxenes (no rims).

[19] Clinopyroxene trace element variations with Mg# are scattered but show general positive trends for compatible elements (e.g., Ni and Sr) and broad negative trends for incompatible trace elements (e.g., REE) (Figure 5). As is the case for both whole-rock and amphibole Sr concentration data, clinopyroxenes from Western and Central domes have markedly higher Sr concentrations than clinopyroxene from the other domes.

4.1.4. Orthopyroxene

[20] Two populations of orthopyroxene phenocrysts are observed with Mg# = 64–82 and Mg# = 46–52 (not shown; supporting information). The higher Mg# population has a similar Mg# range and is in equilibrium with the main clinopyroxene population (Mg# = 68–82), according to the Fe-Mg exchange method of *Putirka* [2008]. Low Mg# orthopyroxene is only present in Breached and Hipaua domes and is not in equilibrium with coexisting clinopyroxene. Due to the low incompatible trace element abundances of orthopyroxene, LA-ICP-MS trace element analysis was not conducted on this mineral.

4.1.5. Plagioclase

[21] Plagioclase major element compositions fall within a field of $Ab_{0–75}Or_{0–15}An_{20–100}$, with a main mode around $An_{20–50}$ for all domes with plagioclase with An contents over 50% making up less than 10% of the data set. High anorthite ($>An_{70}$) plagioclase is only present in Trig M, Hipaua, and Breached dome samples.

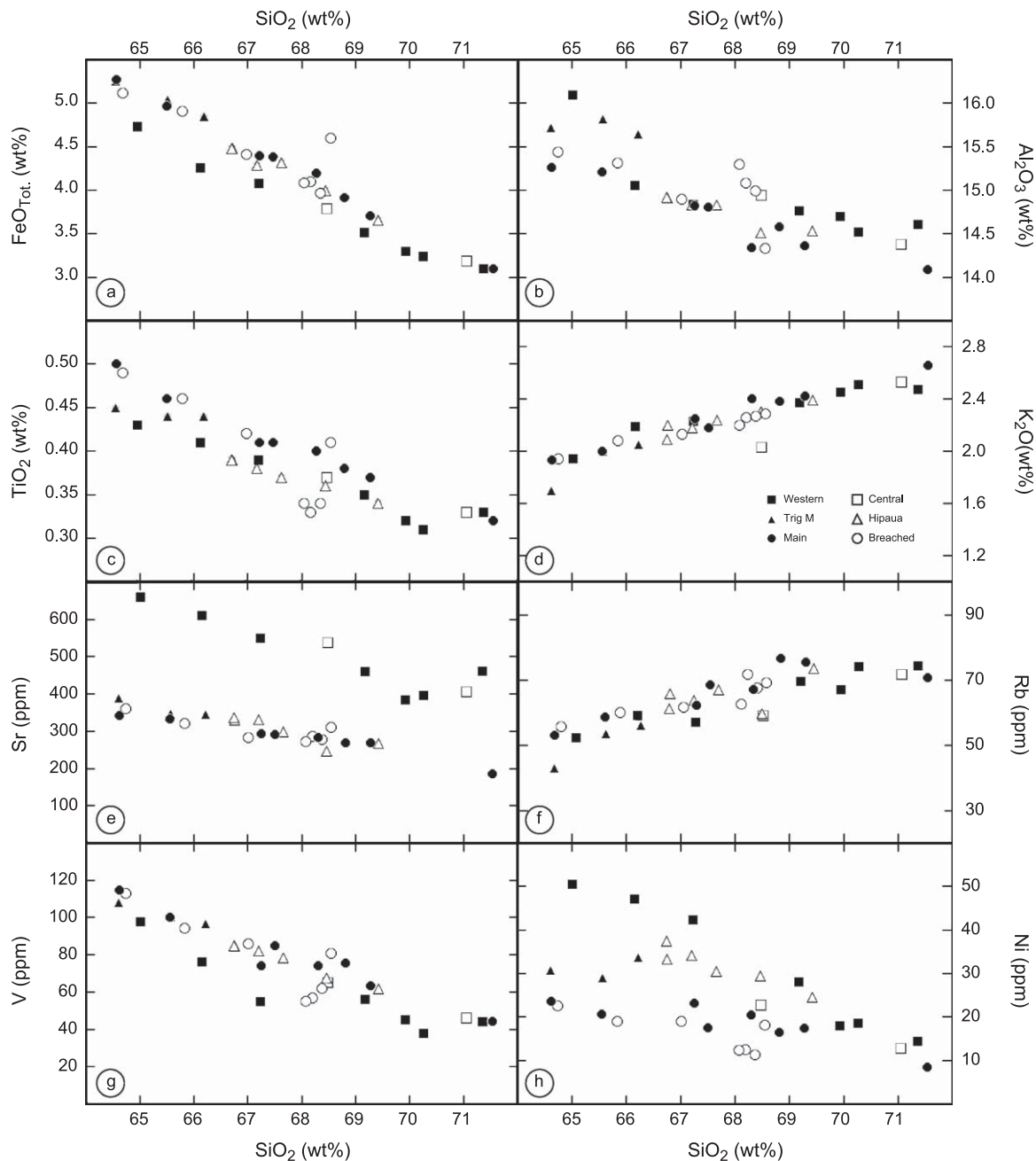[22] Plagioclase trace element concentrations are plotted versus anorthite content (An#) in Figure 6.

Figure 3. Selected plots of major and trace element data versus SiO_2 content for the Tauhara dacites. Data for all samples define strongly linear trends. Note the steep negative trend in plots of V and Ni versus SiO_2, as well as the presence of dome-specific trends in plots of Sr and Ni versus SiO_2.

Sr concentrations shows a positive correlation with An#, whereas Ba, Eu (not shown), and Pb correlate negatively with An#. Unlike the systematic dome differences in Sr concentrations observed in whole-rock and amphibole and clinopyroxene mineral data, there are no clear differences in plagioclase Sr concentrations between domes.

4.1.6. Quartz-Hosted Melt Inclusions

[23] Major and trace element data for quartz-hosted melt inclusions are shown in Figure 7, and the full data set is available as supporting information. SiO_2 contents range between 75.5 and 80.7 wt % for all melt inclusions. Western, Central, and Trig M dome inclusions have SiO_2 = 75.5–79.4 wt % and K_2O > 4.7 wt %. Inclusions from Main and
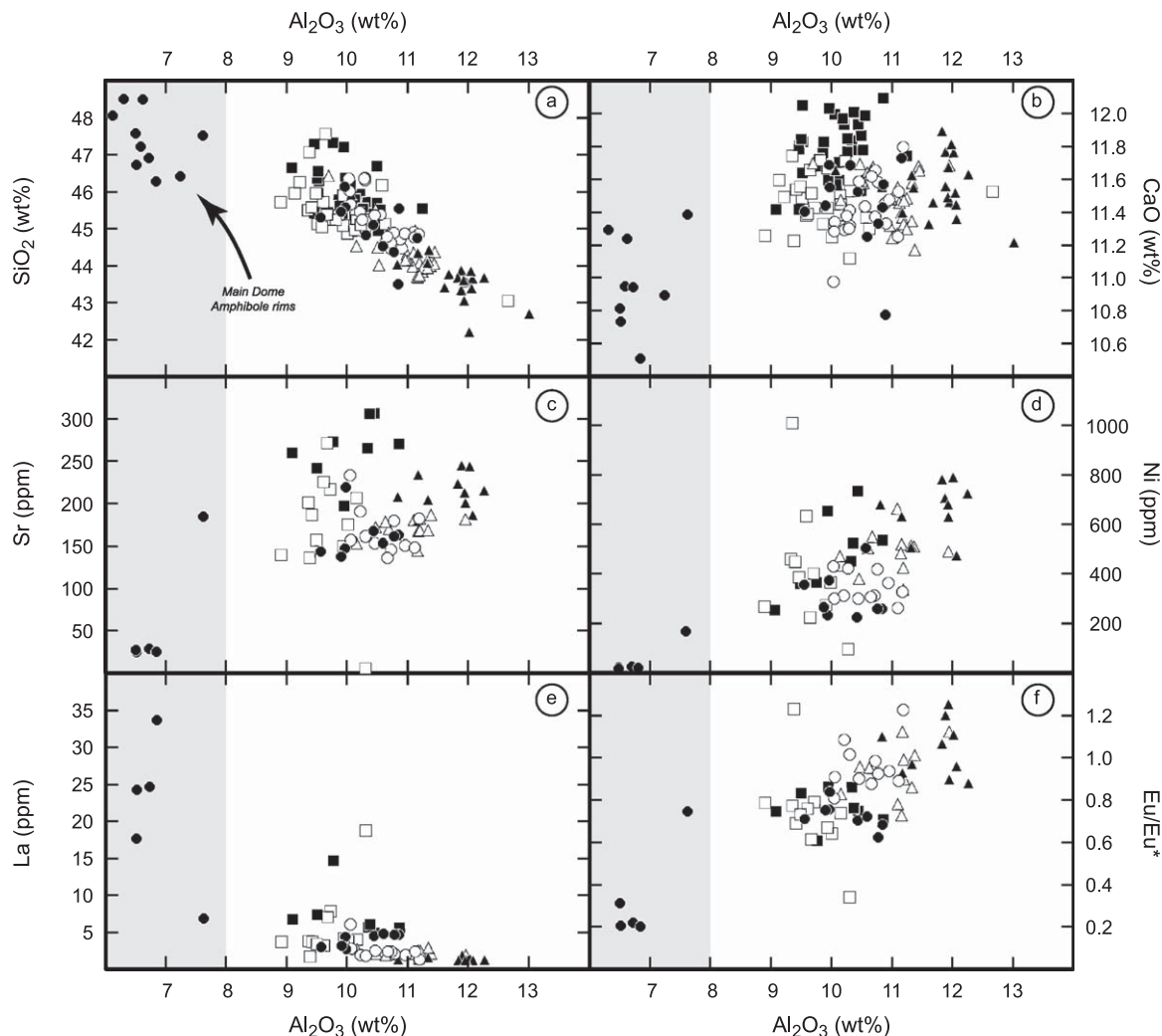
Figure 4. Selected plots of major and trace element data versus Al_2O_3 for amphibole in the Tauhara dacites. Symbols as for Figure 3 and data for cores and rims have identical symbols. Amphiboles from all domes form two populations, with one predominant at high Al_2O_3 and a minor group at low Al_2O_3 comprising data for Main dome amphibole rims and some cores. Note that Sr and Ni data for amphibole from the different domes mimic the differences observed for these elements in the whole-rock data set.

Breached domes have $SiO_2 = 77.5–80.7$ wt %. These inclusions are compositionally distinct from those in the other domes, with $K_2O < 4.6$ wt %. In contrast, the distinct populations of melt inclusions apparent from SiO_2-K_2O systematics show no clear differences in their Al_2O_3, MgO, TiO_2, FeO-$_{Tot}$, and CaO data.

[24] The single Hipaua melt inclusion that we were able to measure also displays a distinct composition, with a SiO_2 content of 79.4 wt % and higher Al_2O_3 than any other quartz-hosted melt inclusions from the Tauhara dacites. This inclusion also has the lowest K_2O content of the suite of analyzed inclusions.

[25] Due to the small size of the inclusions, trace element concentrations could only be analyzed for Western, Central, and Main dome inclusions, which had diameters >15 µm. No systematic differences were observed in the trace element data, although this may reflect the relatively small number of inclusions analyzed for trace elements.

4.2. Sr-Pb Isotope Data

[26] Groundmass Sr-Pb isotope data are presented in Figure 8. Pb isotopic data define a linear array on a plot of $^{208}Pb/^{204}Pb$ versus $^{206}Pb/^{204}Pb$, with
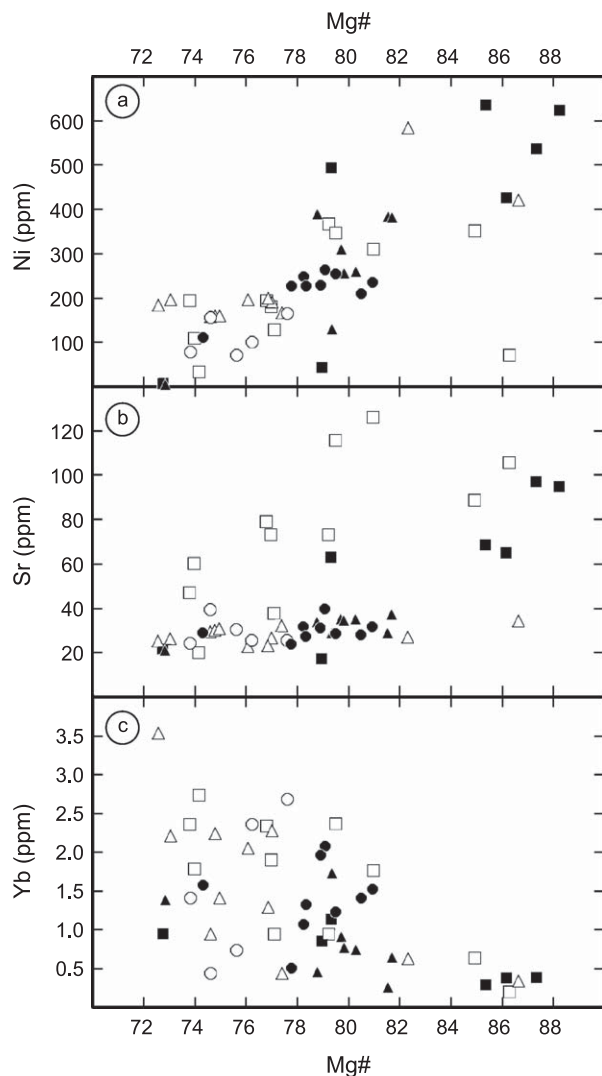
Figure 5. Selected plots of trace element data plotted versus Mg# for clinopyroxenes in the Tauhara dacites. Symbols as for Figure 3. Broad covariations are observed between (a) Ni, (b) Sr, and (c) Yb and Mg#. Clinopyroxene from Western and Central domes tend to have higher Ni and Sr contents than clinopyroxene from the other domes at a similar Mg#, especially for Mg# >80.

[27] Sr-Pb isotope analyses were carried out on individual large plagioclase crystals with c axes > 2 mm in length and pooled small whole plagioclase crystals with c- axes < 1 mm in length (in order to obtain sufficient Sr-Pb for MC-ICP-MS analysis). Plagioclase Pb isotope data reveal that all the plagioclase phenocrysts have more radiogenic Pb and Sr than the groundmass. Although the analytical uncertainties for the individual plagioclase crystal analyses are relatively large, the difference between the plagioclase and dacite data is larger than analytical uncertainties.

[28] Figure 9 shows $^{87}Sr/^{86}Sr$ isotope data for whole rock, groundmass, and all analyzed mineral phases for representative dome samples. Small bulk plagioclase phenocrysts (<1 mm) and large
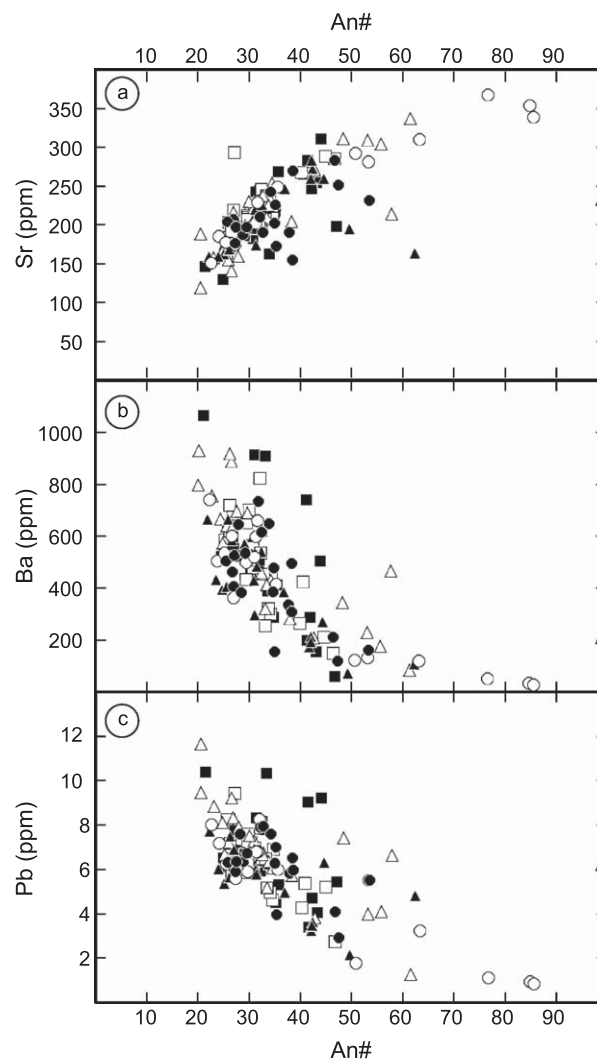

Figure 6. Selected plots of trace element data plotted versus plagioclase An content. Symbols as for Figure 3. Unlike other mineral trace element data, no clear interdome differences in plagioclase trace element chemistry are evident.
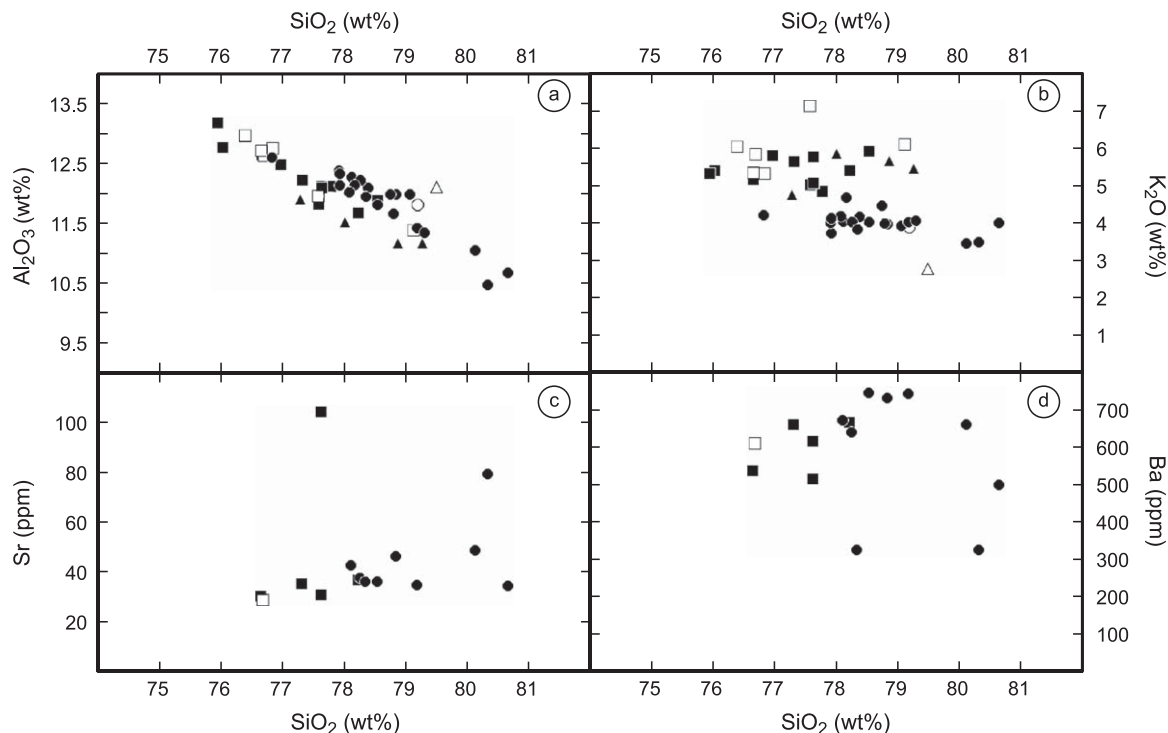
all domes broadly following the same trend. This trend is also observed for $^{207}Pb/^{204}Pb$ versus $^{206}Pb/^{204}Pb$. However, groundmass Sr isotope ratios appear to show two separate populations independent of $^{206}Pb/^{204}Pb$ with groundmass from Western and Central domes having $^{87}Sr/^{86}Sr = 0.7042–0.7046$, whereas groundmass from Main, Breached, Trig M, and Hipaua domes have higher $^{87}Sr/^{86}Sr$ ($^{87}Sr/^{86}Sr = 0.7047–0.7052$) with a single Main dome outlier within the Western and Central dome data at $^{87}Sr/^{86}Sr = 0.7043$.

Figure 7. Selected plots of major and trace element data versus SiO_2 content for quartz-hosted melt inclusions in the Tauhara dacites. Symbols as for Figure 3. Although the melt inclusions do not show any interdome trace element differences, they can be grouped according to (a and b) Al_2O_3 and K_2O contents. Melt inclusion data appear to form four dome groupings: Western and Central; Trig M; Hipaua; Breached and Main domes.

individual plagioclase phenocrysts (>2 mm) plot within the rhyolite fields as represented by data for TVZ rhyolite tephra collected from Ocean Drilling Program (ODP) site 1123 [*Allan*, 2008] and plagioclase from rhyolites erupted from the Maroa Caldera [*McCulloch et al.*, 1994]. Clinopyroxene and amphibole separates yield $^{87}Sr/^{86}Sr$ ratios that are intermediate between those for groundmass and plagioclase for Western, Central, Hipaua, and Main domes. In contrast, amphibole and clinopyroxene from Breached and Trig M domes have almost the same $^{87}Sr/^{86}Sr$ as the groundmass from these domes. Unfortunately, there was insufficient amphibole in the Central dome samples for Sr isotope analysis.

4.3. Thermobarometry, Oxybarometry, and Hygrometry

[29] Temperatures, pressures, oxygen fugacities, and melt water contents for representative samples of the six domes were calculated using the amphibole methods of *Ridolfi et al.* [2010] and *Ridolfi and Renzuli* [2012] (see supporting information). Figure 10 shows temperature versus depth for core

and rim analyses of calc-alkaline amphiboles from Tauhara volcano, whose compositions are close to the data set on which these models were calibrated. Both models give similar pressures, yet temperatures obtained for the main population of amphibole data with the *Ridolfi and Renzulli* [2012] model are consistently 40–50° lower than those from the *Ridolfi et al.* [2010] model (Figure 10a). In both sets of results, apparent crystallization pressures and temperatures recorded by amphiboles from the Tauhara dacites are similar for cores and rims, apart from Main dome, and appear to identify four separate groups consistent with those revealed by major and trace element whole-rock and quartz-hosted melt inclusion data. In the following, we use the results given by the *Ridolfi and Renzuli* [2012] model as it also allows us to recalculate the composition of the melt in equilibrium with the amphibole data. Western and Central dome amphiboles were formed at similar depths of 8.2 ± 0.9 km (1σ; n = 32) and 8.2 ± 0.8 km (1σ; n = 25). Hipaua dome amphiboles were formed at an average depth of 10.5 ± 1.5 km (1σ; n = 25), which is only slightly shallower than Trig M dome amphiboles that crystallized at a depth of 13.1 ± 1.8 km (1σ;
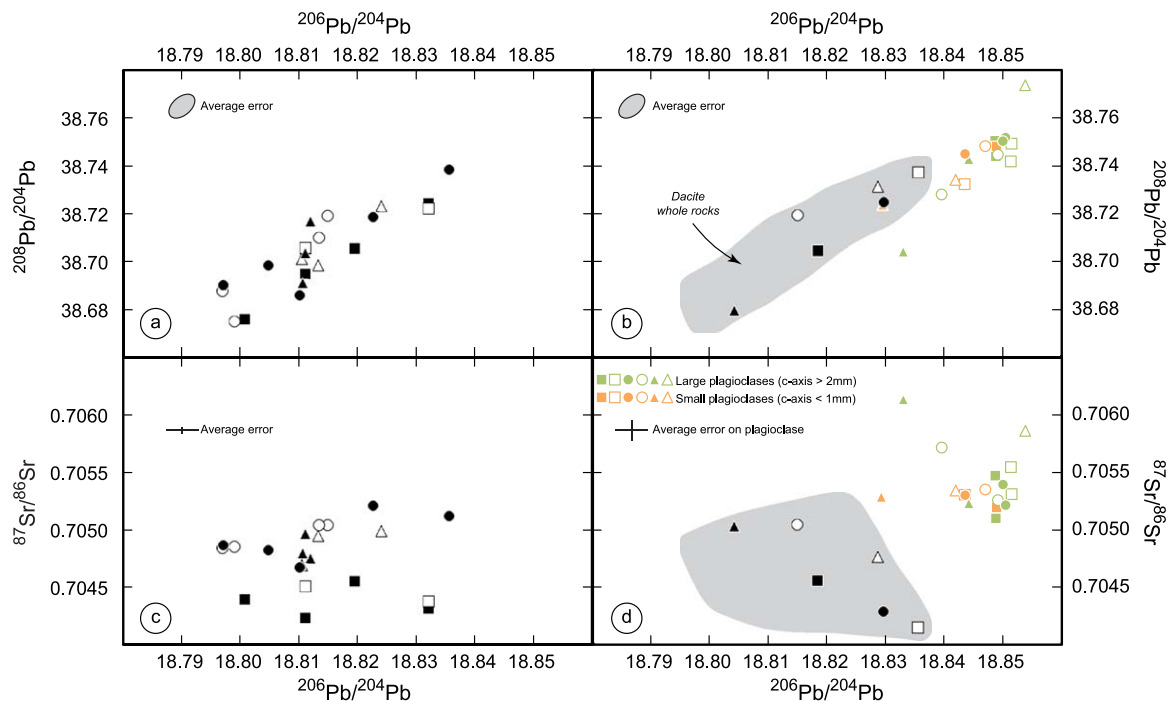
Figure 8. $^{208}Pb/^{204}Pb$ and $^{87}Sr/^{86}Sr$ plotted versus $^{206}Pb/^{204}Pb$ for (a and c) Tauhara dacite whole-rocks and (b and d) handpicked groundmass and plagioclase separates. Error bars for whole-rock/groundmass samples are smaller than the symbol size. Whole-rock data plot on a single mixing trend in Pb isotope space, whereas no clear trend is observed in the Sr-Pb isotope diagram. Data for samples from Western and Central domes plot at lower $^{87}Sr/^{86}Sr$ than data for samples from the other domes at a given $^{206}Pb/^{204}Pb$. Plagioclase and groundmass separates have significantly different Pb-Sr isotopic compositions. Data for groundmass separates always plot within the field defined by whole rocks, whereas plagioclase has systematically more radiogenic Sr-Pb.

n = 20). All Breached dome and high Al# Main dome amphibole cores record similar depths of 9.7 ± 0.8 km (1σ; n = 20) and 9.0 ± 1.0 km (1σ; n = 11), respectively. Some Main dome amphibole cores and all Main dome amphibole rims with low Al# crystallized at much shallower depths of 4.1 ± 0.5 km (1σ; n = 10). However, the apparent pressures obtained from Main dome amphibole rims (100–140 MPa) are slightly outside the Ridolfi and Renzuli's model calibration range, despite having an appropriate chemistry for use with this thermobarometer. As such, the modeled pressures and temperatures for these rims can only be considered a qualitative estimate.

[30] Apparent temperatures recorded by amphiboles follow the same pattern as the calculated depths, albeit with slightly larger scatter. Two-pyroxene thermometry was carried out on samples from Hipaua, Trig M, Breached, and Main domes using the methods of *Putirka* [2008]. The lack of orthopyroxene in samples from Western and Central domes prevented the use of this method for those samples. Two-pyroxene temperatures range from 850 to 1050°C, with most pyroxene rim pairs

recording similar temperatures to those obtained from amphiboles of the same domes (supporting information). In contrast to amphibole thermometry, pyroxene temperatures generally show differences between core and rim temperatures, with rim temperatures being more homogeneous and similar to amphibole temperatures.

[31] Fe-Ti oxide thermometry was also carried out on oxides in the groundmass and inclusions in amphibole and pyroxene phenocrysts using the Ghiorso and Evans thermometer (2008) and equilibrium tested with the Mg-Mn test of *Bacon and Hirschmann* [1988]. Fe-Ti oxides exhibit a range of temperatures similar to the two-pyroxene temperatures, albeit shifted toward lower temperatures (690 to 900°C; supporting information). Groundmass Fe-Ti oxides also tend to yield higher temperatures than those calculated from Fe-Ti oxide inclusions in mafic minerals.

[32] Oxygen fugacities calculated for all the samples using the *Ridolfi and Renzuli* [2012] model do not vary between domes and cluster around the NNO + 2 buffer. Melt water contents obtained
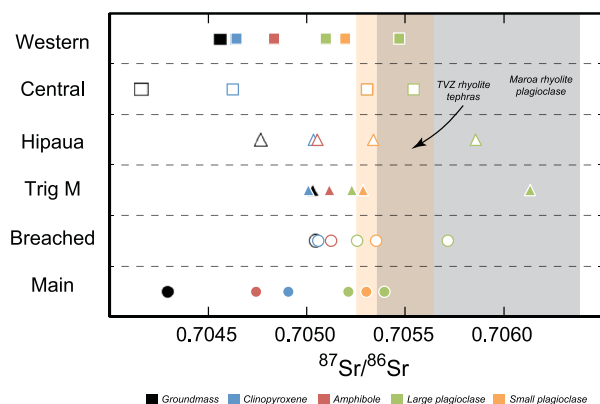
Figure 9. Sr isotope data for minerals and groundmass from each dome. Small (*c* axis < 1 mm) and large (*c* axis > 2 mm) plagioclase crystals have the most radiogenic Sr, and plot in the field of TVZ rhyolite tephras [*Allan*, 2008] and plagioclase from Maroa rhyolite [*McCulloch et al.*, 1994]. Amphibole and clinopyroxene have Sr isotope data closer to the groundmass compositions and are typically intermediate between plagioclase and groundmass data. The Sr isotopic diversity indicates that the crystal cargo in Tauhara dacites did not solely crystallize in the dacitic melt, but was variably inherited during the mixing events from the magma mixing end-members.

from amphibole chemistry broadly correlate with temperature and range from 6.0 to 7.5 wt %, with Hipaua and Trig M domes having the highest calculated water contents. Main dome amphibole rims yield significantly lower water contents of 4.5–5.0 wt % as compared with the other amphiboles.

5. Discussion

5.1. Whole-Rock Geochemical and Isotopic Variations

[33] All major and trace elements define marked linear trends with silica content (Figure 3) and Pb isotopes (Figure 11), which indicates that mixing processes controlled the formation of dacitic magmas at Tauhara volcano, in agreement with previous interpretations [*Graham and Worthington*, 1988]. In addition, the observed textural and isotopic disequilibrium of crystal phases, the highly silicic composition of the quartz-hosted melt inclusions, as well as their position at the extremity of the whole-rock chemical trends defined by the Tauhara dacites indicates that the mixing process involved magmas of different chemical compositions, rather than mixing of a dacitic or rhyodacitic melt with various amount of a crystal

cargo that grew in equilibrium with that melt. Interestingly, whole-rock Sr isotope data do not covary with either major or trace element or Pb isotope data. Sr and Pb have contrasting compatibility in plagioclase with Pb being moderately incompatible whereas Sr is compatible in intermediate and differentiated magmas [*Ewart and Griffin*, 1994]. Although both Sr and Pb isotopic compositions of plagioclase differ from those of the whole-rock samples, the Sr budget of the rocks is more strongly affected by varying proportions of plagioclase in the analyzed samples. As such, this makes Pb isotopes a much more efficient tracer of magma mixing than Sr isotopes, which are likely controlled by signatures inherited from large plagioclase crystals in the dacites.

[34] Samples from Western and Central domes, Hipaua dome, Trig M and Breached domes, and Main dome have separate trends for transition
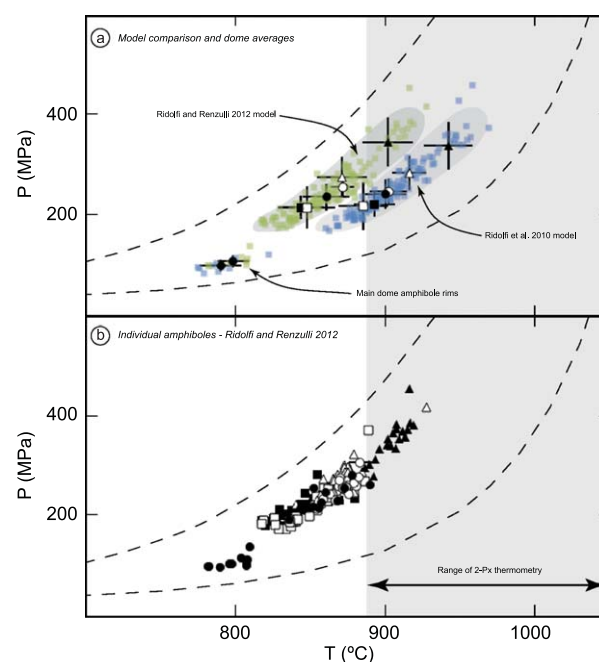

Figure 10. Thermobarometry results obtained from amphibole major element chemistry using *Ridolfi et al.* [2010] (blue squares) and *Ridolfi and Renzuli* [2012] (green squares) models (Figure 10a; including averages for each domes for both models). Both models give equivalent pressures but Ridolfi and Renzuli's models give temperatures that are 40–50° colder on average. Amphiboles from the main population can be divided according to their depth of origin and equilibrium temperature as follows: Western and Central domes (217 ± 23 MPa, 843 ± 15°C; 217 ± 42 MPa, 848 ± 19°C); Hipaua dome (278 ± 41 MPa; 871 ± 16°C); Trig M dome (348 ± 49 MPa; 902 ± 17°C); Breached and Main domes (258 ± 20 MPa, 871 ± 8°C; 238 ± 26 MPa, 861 ± 15°C).

metal (Sc, Cr, Ni, and Cu) and Sr concentration data when plotted against SiO_2 content (Figure 3). This implies that these domes record distinct mixing events. These dome groupings correspond to relative chronological age as well as depths recorded by amphibole barometry and, potentially, hint at four separate mixing events between mafic and silicic magmas.

[35] This relative complexity in terms of the major and trace element systematics contrasts with the single linear array observed in Pb isotope diagrams (Figure 11), although this may simply reflect the very limited range in Pb isotopic compositions (e.g., $^{206}Pb/^{204}Pb = 18.79–18.86$). Pb isotopic data for Tauhara dacites extend from the least radiogenic values recorded by TVZ rhyolites to less radiogenic values that may be a composition intermediate between TVZ basalts and local continental crust (Waipapa and Torlesse terranes; Figure 11c). This suggests that the mafic magma end-member(s) involved in mixing had already been modified by interaction with crust prior to mixing with silicic magmas.

5.2. Mixing End-Member Compositions Evident From Mineral Chemistry

[36] The Tauhara dacites are characterized by a diverse petrographic assemblage comprising clinopyroxene, orthopyroxene, amphibole, plagioclase, and quartz with trace amounts of olivines and Fe-Ti oxides. Disequilibrium textures such as strong mineral zoning, sieved textures or reaction rims [*Graham and Worthington*, 1988] indicate that part of the crystal cargo was not formed in the dacite melt, but was introduced from the mafic and silicic magma mixing end-members. As such, the crystal cargo can reveal specific information regarding the composition of the melt they originated from and the physical conditions that occurred during mixing.

5.2.1. Quartz and Plagioclase Origins
[37] The presence of quartz as well as the fact that quartz-hosted melt inclusions all have $SiO_2 = 76–80$ wt % imply that the quartz crystals formed in a rhyolitic magma. Small differences in the major element chemistry of melt inclusions also potentially identify the presence of at least two separate rhyolitic magmas. However, major element variations in melt inclusions may be partly controlled by fractional crystallization of the melt immediately prior to entrapment, which may overprint initial differences in melt chemistry and the potential

for identifying additional distinct rhyolitic magmas.

[38] All of the analyzed plagioclase crystals have Sr-Pb isotopic compositions that are significantly different to that of their host dacitic groundmass. Data for these plagioclase phenocrysts plot in the field of TVZ rhyolites defined by rhyolitic tephras [*Allan*, 2008] and Maroa rhyolite plagioclases [*McCulloch et al.*, 1994], suggesting that plagioclase, along with quartz, largely originated from a rhyolitic magma. Using plagioclase-melt partition coefficients calculated with the method of *Blundy and Wood* [1991], it is possible to estimate the Sr and Ba contents of the melt in equilibrium with the plagioclase crystals (Figure 12). Sr and Ba plagioclase-melt Kd are temperature dependent. Due to the lack of a temperature estimate for the silicic end-member, assumed temperatures for plagioclase crystallization were those modeled from amphibole thermobarometry (840–900°C). Sr and Ba contents of the melt in equilibrium with plagioclase crystals (see supporting information for values) overlap the field defined by quartz-hosted melt inclusions, whereas whole-rock samples have much higher Sr contents (Figure 12). While the plagioclase crystallization temperature estimate of 840–900°C is likely to be too high for a rhyolite melt, errors associated with temperatures would only result in an overestimate of the Ba content by <20 ppm per 100°C and an underestimate of the Sr content by ca. 10 ppm per 100°C. These uncertainties are insignificant compared with the Sr-Ba concentration differences between whole-rock data and the melts calculated to be in equilibrium with the plagioclase crystals. As such, we conclude that both quartz and most plagioclase crystals originated from the rhyolitic magma end-members that were mixed with mafic melts to create the Tauhara dacites.

5.2.2. Pyroxene and Amphibole Origins
[39] The lack of Mg# variation between cores and rims in amphiboles (apart from Main dome amphiboles) and in the main population of clinopyroxenes indicates that both these crystal phases have grown in magmas in which chemistry did not drastically change, implying that they predominantly grew in the final mixed magma. The new amphibole-melt parameterization by *Ridolfi and Renzulli* [2012] allows back calculation of the major element composition of the equilibrium melt. Dome averages for back-calculated melts compare well with the bulk composition of their host dacite (see supporting information),
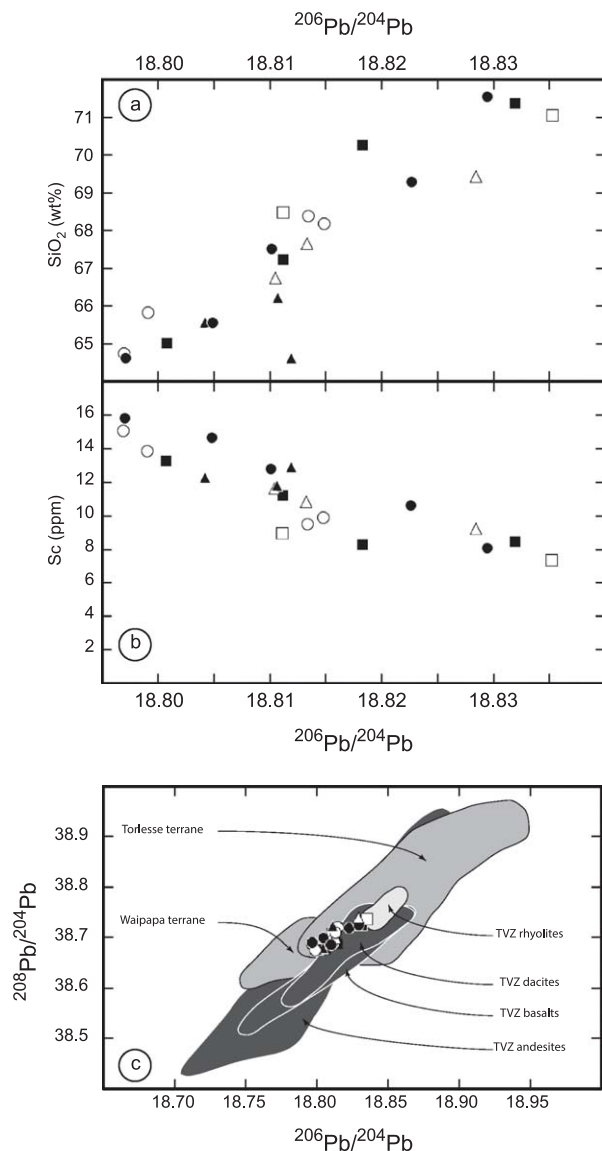
Figure 12. Ba versus Sr concentrations for melts calculated to be in equilibrium with plagioclase, using the methods of *Blundy and Wood* [1991]. Temperatures used for calculation are the average temperatures obtained from amphibole thermometry for each dome. Symbols as for Figure 3. Melt compositions in equilibrium with plagioclase in the Tauhara dacites plot within the range of quartz-hosted melt inclusions, whereas the whole-rock dacites have much higher Sr contents. As such, most of the plagioclase within the dacite can be inferred to have originated from the silicic magma mixing end-members.

Figure 11. Plots of (a) SiO$_2$ and (b) Sc content versus ^{206}Pb/^{204}Pb for the Tauhara dacites. Marked linear trends indicate that the whole-rock chemical and Pb isotope variations are controlled by mixing. (c) Pb isotope data for Tauhara dacites and TVZ basalts, andesites, and dacites (compiled from the georoc database: http://georoc.mpch-mainz.gwdg.de/georoc/), rhyolites [*Allan*, 2008; *McCulloch et al.*, 1994], and Torlesse and Waipapa crustal terranes [*Graham et al.*, 1992; *McCulloch et al.*, 1994]. The Pb isotopic array formed by the Tauhara dacites projects from the TVZ rhyolite field toward data for the crustal terranes, suggesting that mafic magma mixing end-members had already interacted with crustal material prior to mixing with silicic magma mixing end-members.

suggesting equilibrium between most amphiboles and the mixed dacites.

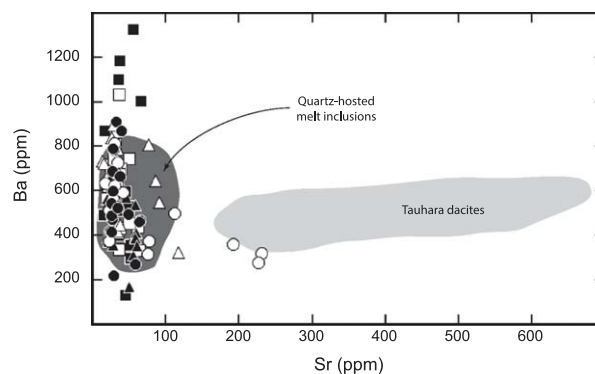[40] Furthermore, REE concentrations of the melts in equilibrium with amphibole and clinopyroxene

can be calculated using dacite-mineral partition coefficients from *Nagasawa and Schnetzler* [1971] and *Sisson* [1994] for amphibole and *Severs et al.* [2009] for clinopyroxene (Figure 13). Back-calculated melts from clinopyroxene and amphibole data, excluding Main dome amphibole rims,
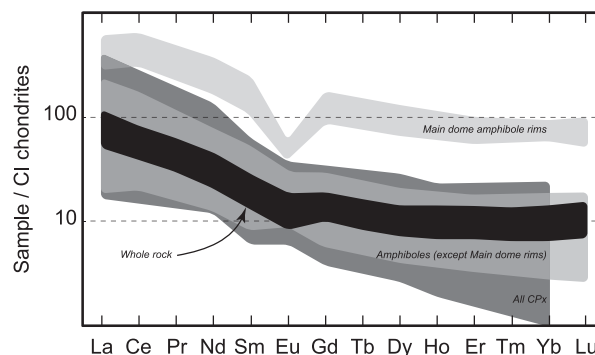

Figure 13. Chondrite-normalized patterns of melt REE concentrations calculated to be in equilibrium with clinopyroxene and amphibole. Mineral-melt partition coefficients were taken from *Severs et al.* [2009] and chondrite normalization values are those of *McDonough and Sun* [1995]. Melts in equilibrium with amphibole have REE concentrations similar to those of the Tauhara dacites, suggesting that amphibole mainly crystallized in the dacite magma after mixing. Most clinopyroxene are also in equilibrium with the Tauhara dacite REE composition, although some clinopyroxenes have lower REE contents suggesting that they originated from the mafic magma mixing end-member.

have REE contents similar to whole-rock data. Together with the major element and Sr isotope data, this suggests that both amphibole and clinopyroxene mainly crystallized in the dacitic melt after mixing. Nevertheless, the field of back-calculated melts in equilibrium with clinopyroxene also marginally extends to lower REE concentrations than the whole-rock dacite data. This indicates that part of the clinopyroxene cargo may have crystallized in a more primitive melt representing the mafic magma mixing end-member(s).

[41] Main dome amphibole rims yield equilibrium melts with highly enriched REE compositions and large negative Eu anomalies compared with whole-rock data that might be the result of an inappropriate choice of partition coefficients. However, hornblende-rhyolite partition coefficients from *Sisson* [1994] yield equilibrium melts that still have higher heavy REE contents than quartz-hosted melt inclusions (not shown). Conversely, this discrepancy can be explained by the effect of lower pressure on trace element partitioning in amphiboles. Experiments conducted by *Green and Pearson* [1985] in andesitic liquids show that trivalent REE become more compatible with decreasing pressure (a factor of 2–3 increase from 12 to 7 kbar), whereas Eu amphibole-melt partitioning remains relatively constant. Although this difference in partition coefficient with pressure is not large enough to explain the REE content in Main dome amphibole rims, the pressures investigated during these experiments are higher than those recorded by Tauhara amphibole barometry and indicate a general trend that is consistent with our data. In addition, the composition of the melt in equilibrium with Main dome amphibole cores calculated using the *Ridolfi and Renzulli* [2012] model matches the composition of the host dacite (sample 527; supporting information). This implies that Main dome amphibole cores crystallized in the final erupted magma and, consequently, the rims of these crystals must have as well.

[42] The above discussion highlights the relative scarcity of amphibole trace element partition coefficients in intermediate magma at relatively low pressures and temperatures in the literature. Given that amphiboles in Tauhara dacites are in equilibrium with the melt, our data set allows us to calculate amphibole-melt partition coefficients from 100 to 350 MPa (see supporting information for calculation details). Transition metals (Sc, V, Cr, Ni, Zn, etc.) as well as Eu were excluded from this calculation because they provided unreliable estimates. Figure 14 shows the results obtained for Zr
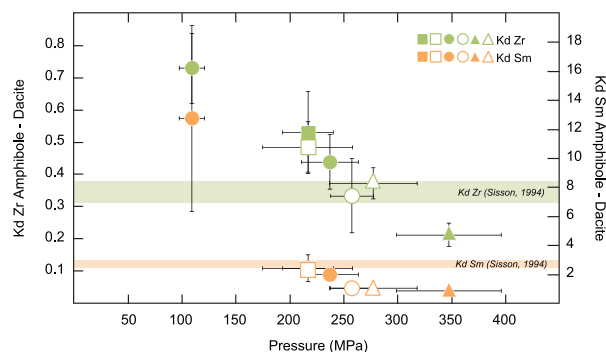

Figure 14. Plot of Zr and Sm amphibole-dacite partition coefficients versus pressure. Amphibole-melt Kds were calculated from amphibole trace element contents (averaged per dome and population) measured in Tauhara dacites. Pressures associated with each data point are apparent pressures obtained by amphibole thermobarometry using the *Ridolfi and Renzulli* [2012] model. These data highlight the strong control of pressure on amphibole partition coefficients at shallow crustal levels (4–13 km depth). Amphibole-dacite partition coefficients from *Sisson* [1994] obtained at 200 MPa are shown for comparison.

and Sm as a function of apparent pressure. At pressures of 200–250 MPa, these compare well with the partition coefficients measured by *Sisson* [1994], which were obtained at 200 MPa and 1050°C. In general, trivalent and tetravalent ions (REE, Y, Zr, Nb, Hf, and Ta) have an increased affinity with amphibole when pressure (and temperature) decreases, whereas divalent ions (Rb, Sr, Ba, and Pb) as well as Th and U, do not show any relationship with pressure (and temperature) with respect to our uncertainties. This is consistent with trends previously observed at higher pressures (0.5–2.5 GPa) by *Adam and Green* [1994] and *Dalpé and Baker* [2000] in basaltic-basanitic melts. These observations add to our understanding of amphibole-melt trace element partitioning of *Tiepolo et al.* [2007], which identified melt chemistry and polymerization as the main control on amphibole-melt Kd for most elements. Our data suggest that pressure is potentially a strong second-order control on trace element partitioning in amphibole, particularly in shallow crustal environments (<13 km).

5.2.3. Determining the Magma Mixing End-Member Compositions

[43] Major and trace element contents of whole-rock dacite samples from Tauhara volcano can be explained by four separate mixing events, each involving mafic and silicic melts of slightly different compositions.

[44] The silicic magma end-member composition is constrained by the chemistry of quartz-hosted melt inclusions. Melt inclusion data generally plots at the end of linear arrays extrapolated through the Tauhara dacite data in element plots versus SiO_2. Exceptions to this are K_2O-Zr and Na_2O that have melt inclusion concentrations that are too high and low, respectively, to plot within the 95% confidence interval envelope of the regression lines passing through the dacite analyses (not shown). This discrepancy may reflect the fact that the quartz-hosted melt inclusions captured variably evolved interstitial melt in a mush zone at the root of a rhyolitic magma chamber due to localized crystallization of zircon and low An-content plagioclase.

[45] Given the absence of primary melt inclusions in the ferromagnesian minerals, the chemistry of the mafic end-members can be examined with two approaches. First, microcrystalline comagmatic enclaves and xenoliths present within the host dacites [*Worthington*, 1985; *Cole et al.*, 2001] can potentially record the chemistry of the intruding mafic magma. However, although these samples generally have andesitic compositions that could be consistent with a mafic end-member, their Sr and REE contents are too low and have been interpreted to represent fragments of crystal mush representing assimilated magma chamber wall rock [*Cole et al.*, 2001]. Here, we use a second approach, utilizing clinopyroxene chemistry. Clinopyroxenes in the Tauhara dacites exhibit a range of Mg# from 72 to 90 that are negatively correlated with heavy REE and positively correlated with Ni contents (Figure 5). Together with the fact that that highest Mg# recorded corresponds to clinopyroxene cores, this indicates that they crystallized in equilibrium with the mafic magma end-members. Using clinopyroxene-melt partition coefficients, it is possible to estimate the trace element compositions of the mafic magma mixing end-members involved in each mixing event. These trace element constraints can, in turn, be used to define the major element composition of the mafic magma mixing end-members using the linear arrays defined by the whole-rock major and trace element data. It is notable that this method can potentially be biased by resorption of the most magnesian clinopyroxene during mixing or by not being analyzed due to their relative rarity. As such, the true composition of the mafic end-members could be even more mafic than those estimated from our data set. A limitation of this approach is that the multiple calculation steps result

in relatively large propagated uncertainties. In order to limit the error propagation for these calculations, we focused on the Sr content of clinopyroxene as it is present in relatively high concentrations in clinopyroxene (20–100 ppm), the uncertainty on the clinopyroxene-melt Sr partition coefficient is small compared with other incompatible elements (e.g., Zr and REE) or transition metals (e.g., V and Sc), and as the mixing trends in a plot of Sr versus SiO_2 diagram are steep (Figure 3). The choice of the clinopyroxene-melt Sr partition coefficient is dependent on the assumed melt chemistry in equilibrium with the clinopyroxene. We used the partition coefficient of *Zajacz and Halter* [2007] that is for a SiO_2 melt content of ca. 57 wt %, which is likely to be close to that of the inferred mafic magma mixing end-members. After initial results showed that the mafic end-member composition for the Western-Central dome mixing event was largely different to the melt composition used by *Zajacz and Halter* [2007] in their experiments, we used a Kd obtained by *Sobolev et al.* [1996] for a basaltic melt and clinopyroxene with a composition matching that of the crystal used in this calculation.

[46] The range of Sr concentrations of the melt calculated to be in equilibrium with clinopyroxene was calculated by taking into account the error on the Sr partition coefficient (0.065 ± 0.005 for Zajacz and Halter; 0.071 ± 0.004 for Sobolev et al.) and then projected onto the best fit line through data for the Tauhara dacites. Other major element abundances (TiO_2, Al_2O_3, Fe_2O_3, MnO, MgO, and CaO) of the mafic magma mixing end-members were then determined using the trends formed in plots of major elements versus SiO_2. Despite their potential to better define regression lines for each mixing array, quartz-hosted melt inclusion data were omitted from the calculations as their K_2O and Na_2O contents do not appear to be strictly representative of the exact composition of the silicic magma mixing end-members involved in the mixing processes. Finally, we note that the small number of samples from Trig M and Hipaua domes have potential for inducing a large bias in estimating the composition of their mafic magma mixing end-member. Given that data for these domes fully overlap those for samples from Breached and Main domes in plots of Sr and major elements versus SiO_2, we used a single regression line for these three mixing events.

[47] Figure 15 shows the results of the mafic magma mixing end-member Sr calculations and their inferred SiO_2 contents for Western-Central and Main-Breached domes (other domes are not shown for the sake of clarity). Major element
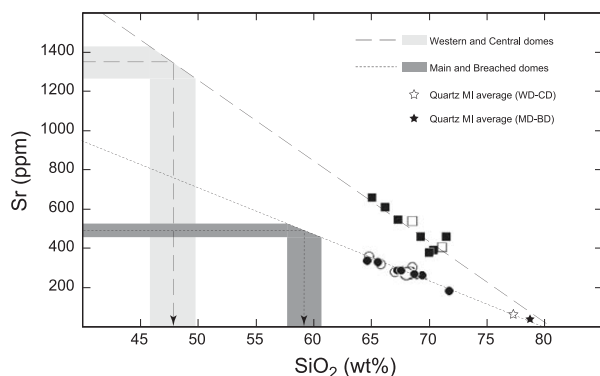
Figure 15. Sr versus SiO₂ plot used to estimate the SiO₂ content of the mafic magma mixing end-members of Western-Central and Breached-Main domes (Hipaua and Trig M domes not shown). The Sr content of melt in equilibrium with the clinopyroxene with the highest Mg# was first estimated using the clinopyroxene-melt partition coefficient of *Zajacs and Halter* [2007] (0.065 ± 0.005) for andesite composition and that of *Sobolev et al.* [1996] (0.071 ± 0.004) for basaltic composition. This value was then projected onto the extension of the best fit line through the dacite data for each mixing event. Concentrations of other major elements were estimated in a similar fashion. Compositions of the mafic mixing end-members for Hipaua, Trig M, Breached, and Main domes were estimated using the same best fit line as the data for samples from these domes are indistinguishable in these diagrams.

compositions of the calculated magmas are listed in Table 2. The mafic magma mixing end-member for Western and Central domes is a high-alumina basalt, comparable to the most primitive magmas found in the central and northern parts of the Taupo Volcanic Zone [*Gamble et al.*, 1990]. In contrast, the mafic magma mixing end-members for the other mixing events have andesitic compositions ranging from 55 to 59 wt % SiO₂, suggesting that these mafic magmas had experienced significant magmatic differentiation prior to mixing. In addition, the most magnesian dacites from Western and Central domes have significantly lower $^{87}Sr/^{86}Sr$ ratios than the magnesian dacites from the other domes. This implies that the andesitic magma mixing end-members may have previously experienced significant crustal contamination. The observation that Pb isotope data for Tauhara dacites plot on a single mixing trend that does not originate from the TVZ basalt field, but rather a composition intermediate between that of TVZ basalts and local crustal terranes (Figure 11), shows that the compositions of all the mafic magma mixing end-members were modified prior to mixing with the rhyolitic magma mixing end-members.

5.3. Physical Conditions of Mixing

[48] Pressure estimates obtained from amphibole chemistry indicate that magma mixing took place in four different sites located at depths ranging from 8 to 13 km. The crustal thickness under the Taupo Volcanic Zone is estimated to be ca. 16–20 km [*Harrison and White*, 2004; *Stern et al.*, 2010], indicating that dacite formation occurred in the midcrust to lower crust. However, Tauhara volcano is located on the eastern edge of the TVZ where the crust may be thicker and, as such, dacite formation probably took place in the midcrust. It is notable that most rhyolite bodies in the TVZ appear to have formed at shallower depths of 3–10 km [*Brown et al.*, 1998; *Allan et al.*, 2012; *Cooper et al.*, 2012], with recent evidence pointing to a strong link between rhyolite accumulation and extensional tectonics in the TVZ [*Allan et al.*, 2013]. The modeled pressure estimates for the assembly of Tauhara dacites show that rhyolites are also present at deeper levels in the crust beneath the TVZ. Main dome amphibole rims record lower apparent pressures indicating that they crystallized at a depth of ca. 4 km, compared with most amphibole cores, which record depths of ca. 9 km. However, REE concentrations of amphibole cores are in equilibrium with dacitic melt, suggesting that mixing occurred at this depth (ca. 9 km), and that the dacite magma then stalled at 4 km depth *en route* to the surface without further mixing with any other magmas.

[49] Magma temperatures were obtained from three different mineral thermometers: amphibole; Fe-Ti oxides; two-pyroxene (apart from Western and Central domes). For each dome, data from amphibole cores (all domes) and rims (apart from Main dome) yield a relatively narrow range of temperatures (840–900°C) as compared with the other thermometers. This is consistent with the amphiboles being in chemical and isotopic equilibrium with the groundmass and, therefore, recording the dacite magma temperature after magma mixing.

[50] Fe-Ti oxides generally record lower temperatures (690–900°C) than amphibole. This observation is at odds with the accepted fast reequilibration of Fe-Ti oxides with their host melt [*Venezky and Rutherford*, 1999]. However, extensive crystal-melt disequilibrium (such as that observed in Tauhara dacites) leading to instability of silicate phases can affect melt composition at the microscopic scale, which in turn will affect the composition of growing and/or equilibrating Fe-Ti

Table 2. Major Element Composition of the Mafic End-Members Involved in the Formation of Tauhara Dacites[a]

Dome	Western/Central			Hipaua			Trig M			Breached/Main		
	Av.	Low Si	High Si	Av.	Low Si	High Si	Av.	Low Si	High-Si	Av.	Low Si	High Si
SiO_2	48.11	46.15	49.85	57.74	55.86	59.34	55.74	53.69	57.49	59.33	57.58	60.82
TiO_2	0.74	0.77	0.71	0.65	0.69	0.61	0.70	0.75	0.65	0.61	0.65	0.57
Al_2O_3	18.89	19.27	18.55	17.13	17.56	16.76	17.59	18.05	17.19	16.77	17.16	16.43
Fe_2O_3 tot	8.91	9.40	8.46	7.36	7.94	6.86	7.97	8.60	7.43	6.86	7.40	6.40
MnO	0.05	0.04	0.05	0.14	0.15	0.13	0.15	0.16	0.14	0.13	0.14	0.12
MgO	8.13	8.70	7.61	4.84	5.31	4.43	5.34	5.85	4.90	4.44	4.88	4.06
CaO	11.69	12.39	11.06	7.96	8.63	7.39	8.67	9.40	8.05	7.40	8.02	6.87
Na_2O	2.54	2.44	2.63	2.92	2.79	3.03	2.78	2.64	2.90	3.03	2.91	3.14
K_2O	0.55	0.39	0.70	1.10	0.89	1.29	0.88	0.65	1.08	1.28	1.09	1.45
Total	99.59	99.55	99.62	99.83	99.82	99.85	99.81	99.80	99.83	99.85	99.83	99.86
CPx Mg#	88			87			82			81		
f_{max}	0.42			0.59			0.61			0.73		
f_{min}	0.20			0.46			0.54			0.37		

[a]Low Si and high Si correspond to the low silica and high silica estimates for each mafic magma that are obtained when taking into account the error on the Sr partition coefficient in clinopyroxene (see text for further details). f_{min} and f_{max} are the minimum and maximum proportion of mafic magma necessary to explain the chemical variation within dacites belonging to the same mixing event. The Mg# of the clinopyroxene used for the calculation is also indicated.

oxides. This will lead to oxide pairs, despite satisfying the Mg-Mn test of *Bacon and Hirschmann* [1988], yielding anomalous temperatures. As such, we contend that Fe-Ti oxides do not give information regarding the mixing process.

[51] Two-pyroxene thermometry yields temperatures equivalent to or higher than the amphibole temperatures (850–1040°C) with the pyroxene rims giving temperatures most consistent with those from amphibole (840–900°C). This is consistent with the clinopyroxene trace element chemistry of most crystals being in equilibrium with dacitic melts, with some crystals, with high Mg# and Ni contents and low heavy REE contents, interpreted as originating from the mafic magma mixing end-members. We thus infer that pyroxene crystal pairs recording the highest temperatures do not originate from the dacitic melt, but instead represent our best estimate of the mafic magma mixing end-member temperatures (ca. 1050°C).

5.4. Time Scales of Magma Mixing and Ascent

[52] The crystal cargo in the Tauhara dacites displays significant chemical and textural disequilibrium features. Diffusion of elements across zone boundaries in minerals can be used to estimate the time spent by crystals in magmas with which they are not in chemical equilibrium [*Morgan et al.*, 2004; *Costa and Morgan*, 2010]. More specifically, boundaries between Ti-poor cores and Ti-rich rims in quartz crystals most likely reflect their transition from rhyolite magma (i.e., silicic end-

member) in which they initially crystallized to the final mixed dacitic magma. Uncertainties in diffusion coefficients and the resulting time scales for Ti diffusion in quartz are dependent on the temperature at which diffusion is assumed to have taken place. Given that the modeled boundaries reflect the mixing events, the most appropriate temperature estimates are those given by amphibole thermometry.

[53] Model ages were calculated using the one-dimensional model of *Morgan et al.* [2004] with diffusion coefficients from *Cherniak et al.* [2007]. Diffusion ages and diffusion coefficients and their associated errors are given in supporting information and presented in Figure 16. In general, quartz crystals give diffusion ages ranging from 2 month to 2 years. Diffusion time scales estimate the time between the start of disequilibrium conditions (in this case, when quartz crystals and the host rhyolitic melt are mixed with a more mafic magma) and the time at which diffusion stops in quartz crystal, usually the time of eruption. There is a marked difference between the modeled mixing times of Western and Central dome dacites (1–2 years) and those of Trig M, Breached, and Main dome dacites (2–7 months), which mimics the differences already observed in the composition of bulk rocks and mixing end-members.

[54] The shortest time scales recorded in this study are slightly longer than estimates for other mixed dacites at Quizapu volcano (days to weeks) [*Ruprecht and Cooper*, 2012], Ceboruco volcano (1–2 months) [*Chertkoff and Gardner*, 2004], Nea Kamini center (1–2 months) [*Martin et al.*, 2008],
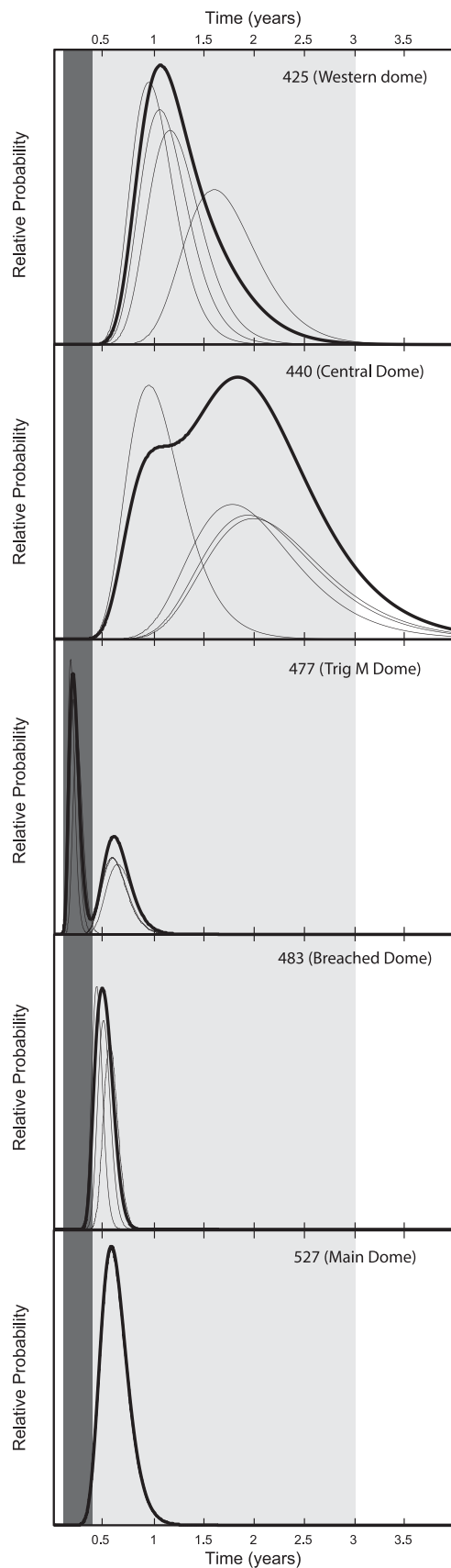
Figure 16.

and the 1991–1995 Mt Unzen eruption (1–5 months) [*Nakamura*, 1995]. In all these systems, the silicic mixing end-member was of dacitic composition, whereas the mafic end-member was either andesitic or dacitic, implying a less important chemical contrast between the two magmas brought into contact than that inferred from our data set. Conversely, *Coombs et al.* [2000] estimated time scales for a range of basaltic andesite-rhyolite mixing events of ca. 1 month to 3 years at Southwest Trident volcano (Katmai, Alaska) using Fe-Mg diffusion in olivine and Fe-Ti in magnetite. These time scales span the entire range found in our study, which may reflect a closer match in mixing end-member compositions in these two settings.

[55] *Mashima* [2004] and *Costa and Chakraborty* [2004] have estimated time scales of dacite assembly by mixing that are significantly different from those discussed above (Saga-Futagoyama dacite = hours to days for the former; Volcan San Pedro = years to decades). However, unlike Tauhara, Quizapu, Ceboruco, Nea Kamini, or Mt Unzen, these time scales may reflect different processes. Saga-Futagoyama dacite assembly occurred during ascent in the conduit [*Mashima*, 2004], not in a well-stirred magma chamber. In the case of Volcan San Pedro, *Costa and Chakraborty* [2004] highlighted the fact that eruption was triggered by flank collapse, not by a recharge event.

[56] Turning to time scales obtained from diffusion of Ti in quartz crystals, most previously published work has focused on constraining the timing of the last stages of rhyolite body assembly [Whakamaru: *Saunders et al.*, 2010; *Matthews et al.*, 2012a, 2012b; Younger Toba Tuff and Earthquake Flat: *Matthews et al.*, 2012b]. The time scales recorded point to mafic recharges ca. 10–200 years before eruption, which is ca. 2 orders of magnitude longer than those recorded for Tauhara dacites. The exact controls on these differences are yet to be explored, but it is expected that

Figure 16. Time scales of Ti diffusion in quartz crystals collected from selected dacites samples. Diffusion time scales were calculated using the 1-D model of *Morgan et al.* [2004] and the diffusion coefficients of *Cherniak et al.* [2007]. Note the longer diffusion times obtained in quartz crystals from Western and Central domes. Shaded areas are mixing time scales obtained for other assembly of other subduction zone dacites: dark gray = Quizapu volcano [*Ruprecht and Cooper*, 2012], Ceboruco volcano [*Chertkoff and Gardner*, 2004], Nea Kamini center [*Martin et al.*, 2008], Mt Unzen 1991–1995 [*Nakamura*, 1995], and light gray = Southwest Trident [*Coombs et al.*, 2000].

Table 3. Estimates of Ascent Rates Based on Amphibole Rim Destabilization[a]

Dome	WD	CD	HD	TD	BD
Average width	18	27	14	19	9
Min width	12	15	9	9	3
Max width	30	39	27	36	24
Average ascent rate (m/s)	0.007	0.005	0.008	0.007	0.010
Max ascent rate (m/s)	0.009	0.008	0.010	0.010	0.013
Min ascent rate (m/s)	0.005	0.004	0.005	0.004	0.006
Average time (days)	14	17	16	22	11
Min time (days)	11	12	13	15	8
Max time (ascent rate (m/s))	19	22	23	34	19

[a]Calculations are based on experiments by *Rutherford and Hill* [1993], and assuming a constant decompression rate between 200 and 2 MPa.

the relative volumes of mafic versus silicic magma involved in each case, and the resultant chemistry of the erupted magma, played a prominent role.

[57] Amphibole rim destabilization is related to the amount of time spent by amphibole outside the hornblende stability field and can, therefore, be used as a proxy for ascent rate and duration [*Rutherford and Devine*, 2002; *Browne and Gardner*, 2006]. Using decompression experiment results from *Rutherford and Hill* [1993] undertaken on compositionally similar dacites from Mt St Helens, it is possible to estimate the duration and rate of ascent of the Tauhara dacitic magmas for all domes but Main dome. Main dome amphiboles do not show signs of destabilization. Estimates of the duration and rate of ascent are summarized in Table 3. Calculations were made assuming a constant rate of decompression between 200 (ca. 7.5 km) and 2 MPa. Magma ascent rates for all domes range from 0.005 to 0.010 m/s, which are comparable to a range of other estimates for dacite eruptions at Black Butte dome (0.004–0.006 m/s) [*McCanta et al.*, 2007], Mt St Helens (0.004–0.020 m/s) [*Rutherford and Hill*, 1993; *Geschwind and Rutherford*, 1995] and Mt Unzen (0.003–0.007 m/s) [*Rutherford*, 2008]. Amphibole rim widths measured in thin sections display a nearly unimodal distribution and a range of variation of ca. 20 μm within each thin section, which is similar to the distribution observed in Black Butte dacites [*McCanta et al.*, 2007]. However, Mt St Helens amphibole rim widths [*Rutherford and Hill*, 1993] have a large range of variations and distributions that are skewed to large rim widths. Skewed distributions have been interpreted to reflect remobilization of older magma that lines ascent conduits, and the absence of these in the Tauhara dacites may suggest that the ascent path for each batch of magma was distinct at Tauhara

volcano. Extrapolating the obtained magma ascent rates to the depth of each dome's magma chambers, results in calculated average ascent times of 14 and 17 days for Western and Central domes, 16 days for Trig M dome, 22 days for Hipaua dome, and 11 days for Breached dome. These time scales for ascent are shorter than the Ti diffusion in quartz time scales for the magma mixing event that produced the dacite magma (2 months to 2 years).

5.5. Mixing Processes and Preferential Eruption of Dacitic Magmas at Tauhara Volcano

[58] One of the striking features of the Tauhara dacites is their petrographic homogeneity and lack of any preferred crystal orientation, which implies that mixing occurred in a well-stirred magma chamber rather than in a narrow conduit during ascent to the surface. Diffusion ages obtained from quartz crystals estimate the time between the onset of mixing and eruption and, therefore, overestimate the magma mixing time scales. These are better estimated by the difference between the diffusion and ascent time scales, which represents the time required to homogenize the silicic and mafic magma mixing end-members into an eruptible intermediate magma. The time lag between onset of mixing and magma ascent are similar for Trig M, Breached, and Main domes (2–7 months), but markedly longer for Western and Central domes (1–2 years).

[59] Magma mixing efficiency is strongly controlled by the viscosity contrast between silicic and mafic magma end-members at equilibrium temperature [*Sparks and Marshall*, 1986]. Viscosity is dependent on melt chemistry and the amount of crystals present in the magma. The Tauhara dacites contain ca. 15%–18% crystals (with an estimated 10% relative uncertainty) of which 9%–10% are plagioclase and quartz from the rhyolite magma and 2%–4% is amphibole and 2.0%–2.5% is clinopyroxene, which largely crystallized in the mixed dacite magma. The proportion of rhyolite magma involved in mixing varies from 70% in Western and Central domes to 40% in Breached and Main domes. Although only qualitative, this implies that the rhyolite magmas were crystal rich, whereas the mafic magmas were all relatively crystal poor. Using a crystallinity of 0%–5% and temperature of 1050°C, the calculated viscosities (using the methods of *Scaillet et al.* [1998] and *Giordano et al.* [2008]) for the andesite magma

involved in the Hipaua, Trig M, Breached, and Main dome mixing events are about 1 order of magnitude greater than those of the basalt (1100°C, 0%–5% crystallinity) involved in the Western-Central dome mixing events (see supporting information for calculation results). This implies that the andesite magma mixing end-members were more readily mixable with the rhyolite magma end-members than the basalt mixing end-members, which most likely explains why longer Ti-in-quartz diffusion time scales characterize Western and Central domes. In a global context, this difference in magma physical properties could explain the differences in time scales recorded in other mixed dacites (Quizapu, Ceboruco, Nea Kamini, and Mt Unzen), where the contrast between end-member chemistries is not as large as those recorded in Tauhara dacites. Interestingly, in the case of Southwest Trident dacites, which are the product of a mixing event equivalent to Western-Central domes, recorded time scales are similar.

[60] Volcanoes that consistently erupt magmas of intermediate composition, such as Tauhara volcano, have been proposed to be reliant on a recharge filtering process [*Kent et al.*, 2010], where silicic and mafic magmas that are either too viscous (silicic) or dense (mafic) to erupt, mix to produce eruptible intermediate magmas. Calculated viscosities for the Tauhara dacites are 3 or 4 orders of magnitude lower than those calculated for the silicic magma mixing end-member using quartz-hosted melt inclusion compositions (800°C; 20% crystallinity). Similarly, densities calculated following the method of *Bottinga and Weill* [1970] and the spreadsheet available at www.gabbrosoft.org of the Tauhara dacites are ca. 10% and 5% lower than the basaltic and andesitic magma mixing end-members, respectively. These contrasts in the physical properties of the magmas involved at Tauhara volcano are consistent with the recharge filtering process governing the nature of the erupted magmas.

[61] In the central section of the TVZ, eruption of dacitic magma primarily occurs near its eastern boundary, as well as in its southern segment, whereas the rest of the central section of the TVZ is largely dominated in terms of both frequency and volume by rhyolitic (super)eruptions [*Wilson et al.*, 1995]. Minor amounts of basaltic magmatism also occurs, usually located at the intersection of major faults and caldera boundaries [*Cole*, 1990]. The regions of the TVZ that erupt dacite are characterized by lower heat flux and may also be undergoing less local crustal extension, param-

eters which have both been suggested to control rhyolitic magma accumulation [*Allan et al.*, 2013] and eruption [*Gravley et al.*, 2007; *Allan et al.*, 2012; *Cooper et al.*, 2012]. This indicates that in regions where tectonic constraints, whether active (high rate of crustal extension, active faults, and high heat flux) or passive (preexisting structural weakening of the entire crust) are lessened or absent, the recharge filtering process is key to the generation of eruptible magmas.

6. Conclusions

[62] A detailed chemical and isotopic study of dacites and their crystal cargo from six domes of Tauhara volcano (Taupo Volcanic Zone, New Zealand) has revealed the processes and time scales responsible for dacite magma genesis and eruption. The main findings of this study are based on mineral-specific investigations and are:

[63] 1. The dacites represent mixed magmas of different mafic and silicic magma end-members. The oldest Western and Central domes result from the same mixing event between ca. 30% of high-alumina basalt (ca. 48 wt % SiO_2) and ca. 70% rhyolite (ca. 77 wt % SiO_2) at depths of ca. 8 km. Hipaua and Trig M domes were produced by two separate mixing events involving subequal proportions (ca. 50%–55%) of andesitic magmas (57 and 55 wt % SiO_2, respectively) with two different rhyolite magmas (low K and high K, respectively). Magma chambers for the Hipaua and Trig M domes were located deeper in the crust (11 and 13 km, respectively). The youngest Breached and Main domes were formed from mixing of ca. 40%–70% andesite (ca. 59 wt % SiO_2) with a low-K rhyolite at depths of 9 km. Main dome magmas stalled for a period *en route* to the surface at depths of 4 km.

[64] 2. Trace element and Sr-Pb isotopic fingerprints of the dacite crystal cargo demonstrate that quartz and plagioclase in the Tauhara dacites originated from the silicic magma mixing end-members, whereas amphibole and clinopyroxene largely crystallized from the mixed dacite, suggesting that mixing occurred between crystal-poor mafic magmas and relatively crystal-rich silicic magmas.

[65] 3. New amphibole-dacite partition coefficients can be calculated for apparent pressures ranging from 100 to 350 MPa (see supporting information for results). They show a strong relationship with pressure-temperature for most elements (REE, Y, Zr, Nb, and Hf) at crustal depth <13 km.

[66] 4. Mixing time scales between the mafic and silicic magma end-members range from 1–2 years (Western and Central domes) to 2–7 months (Hipaua and Trig M domes), with longer time scales characterizing mixing where the end-members have the largest temperature, viscosity, and compositional contrasts (i.e., the basaltic magma mixing end-member of Western and Central domes). Amphibole rim destabilization due to magmatic water loss during ascent indicates that after a period of mixing of 2–24 months the dacite magmas took 2–3 weeks to ascend to the surface.

[67] 5. Calculated viscosities and densities for magmas involved in dacite assembly show that the dacite magma was far more eruptible than either mixing end-member, with densities 5%–10% lower than the mafic mixing end-members and viscosities 3 to 4 orders of magnitude lower than the silicic mixing end-members. Larger proportions of andesitic magma end-members as compared with the basaltic magma end-members were required to mix with the silicic magma end-members to create an eruptible intermediate magma. This gives further credence to the recharge filtering process proposed by *Kent et al*. [2010] to explain volcanoes that consistently erupt magmas of intermediate composition.

[68] 6. Other subduction zone dacites assembled by mixing in well-stirred magma chambers record similar or shorter time scales between mixing and eruption. This appears to be related to the contrast in the chemistry (i.e., their viscosity) of the mixing end-members.

[69] 7. In the central TVZ, intermediate mixed magmas only erupt on the eastern edge, where the heat flux is lower and extensional tectonism is generally less active. This contrasts with the strong tectonic control on rhyolitic-basaltic volcanism in the central TVZ and hints that mixing may be the most favorable way to generate eruptible magmas in tectonically quiescent areas.

[70] 8. The time scales provided in this study for magma mixing and subsequent dacite eruption could be used to assess and mitigate against volcanic risk in the TVZ, if seismic evidence for such magma intrusion into midcrustal silicic magma chambers or crystal-magma mushes can be detected.

Acknowledgments

References

Adam, J., and T. H. Green (1994), The effects of pressure and temperature on the partitioning of Ti, Sr and REE between amphibole, clinopyroxene and basanitic melts, *Chem. Geol.*, *117*, 219–233.

Allan, A. S. R. (2008), An elemental and isotopic investigation of Quaternary silicic Taupo Volcanic Zone tephras from ODP Site 1123: Chronostratigraphic and petrogenetic applications, MSc thesis, Victoria Univ. Wellington, New Zealand.

Allan, A. S. R., C. J. N. Wilson, M.-A. Millet, and R. J. Wysoczanski (2012), The invisible hand: Tectonic triggering and modulation of a rhyolitic supereruption, *Geology*, *40*, 533–566.

Allan, A. S. R., D. J. Morgan, C. J. N. Wilson, and M.-A. Millet (2013), From mush to eruption in centuries: Assembly of the super-sized Oruanui magma body, *Contrib. Mineral. Petrol.*, *166*, 143–164.

Bacon, C. R., and M. M. Hirschmann (1988), Mg/Mn partitioning as a test for equilibrium between coexisting Fe-Ti oxides, *Am. Mineral.*, *73*, 57–61.

Blundy, J. D., and B. J. Wood (1991), Crystal-chemical controls on the partitioning of Sr and Ba between plagioclase feldspar, silicate melts, and hydrothermal solutions, *Geochim. Cosmochim. Acta*, *55*, 193–209.

Bottinga, Y., and D. F. Weill (1970), Densities of liquid silicate systems calculated from partial molar volumes of oxide components, *Am. J. Sci.*, *269*, 169–182.

Brown, S. J. A., C. J. N. Wilson, J. W. Cole, and J. Wooden (1998), The Whakamaru group ignimbrites, Taupo Volcanic Zone, New Zealand: Evidence for reverse tapping of a zoned silicic magmatic system, *J. Volcanol. Geotherm. Res.*, *84*, 1–37.

Browne, B. L., and J. E. Gardner (2006), The influence of magma ascent path on the texture, mineralogy, and formation of hornblende reaction rims, *Earth Planet. Sci. Lett.*, *246*, 161–176.

Carmichael, I. S. E. (2002), The andesite aqueduct: Perspectives on the evolution of intermediate magmatism in west-central (105-99°W) Mexico, *Contrib. Mineral. Petrol.*, *143*, 641–663.

Cherniak, D. J., E. B. Watson, and D. A. Wark (2007), Ti diffusion in quartz, *Chem. Geol.*, *236*, 65–74.

Chertkoff, D. G., and J. E. Gardner (2004), Nature and timing of magma interactions before, during, and after the caldera-forming eruption of Volcán Ceboruco, Mexico, *Contrib. Mineral. Petrol.*, *146*, 705–735.

Cole, J. W. (1990), Structural control and origin of volcanism in the Taupo Volcanic Zone, New Zealand, *Bull. Volcanol.*, *52*, 445–459.

Cole, J. W., and K. B. Lewis (1981), Evolution of the Taupo-Hikurangi subduction system, *Tectonophysics*, *72*, 1–21.

Cole, J. W., J. A. Gamble, R. M. Burt, L. D. Carroll, and D. Shelley (2001), Mixing and mingling in the evolution of andesite-dacite magmas; evidence from co-magmatic plutonic enclaves, Taupo Volcanic Zone, New Zealand, *Lithos*, *59*, 25–46.

Coombs, M. L., J. C. Eichelberger, and M. J. Rutherford (2000), Magma storage and mixing conditions for the 1953–1974 eruptions of Southwest Trident volcano, Katmai

National Park, Alaska, *Contrib. Mineral. Petrol.*, *140*, 99–118.

Cooper, G., C. J. N. W. Wilson, M.-A. Millet, J. A. Baker, and E. G. C. Smith (2012), Systematic tapping of independent magma chambers during the 1 Ma Kidnappers supereruption, *Earth Planet. Sci. Lett.*, *313–314*, 23–33.

Costa, F., and S. Chakraborty (2004), Decadal time gaps between mafic intrusion and silicic eruption obtained from chemical zoning patterns in olivine, *Earth Planet. Sci. Lett.*, *227*, 517–530.

Costa, F., R. Dohmen, and S. Chakraborty (2008), Timescales of magmatic processes from modeling the zoning patterns of crystals, *Rev. Mineral. Geochem.*, *69*, 545–594.

Dalpé, C., and D. R. Baker (2000), Experimental investigation of large-ion-lithophile-element, high-field-strength element and rare-earth-element-partitioning between calcic amphibole and basaltic melt: The effects of pressure and oxygen fugacity, *Contrib. Mineral. Petrol.*, *140*, 233–250.

Davidson, J. P., D. J. Morgan, B. L. A. Charlier, R. Harlou, and J. M. Hora (2007), Microsampling and isotopic analysis of igneous rocks: Implications for the study of magmatic systems, *Annu. Rev. Earth Planet. Sci.*, *35*, 273–311.

Dawson, G. B., and G. E. Thompson (1981), Groundwater survey at Taupo, Part 2: Relationships geophysical, geochemical and geological, geophysics division report 219, Dep. of Sci. and Ind. Res., New Zealand.

Eichelberger, J. C., P. E. Izbekov, and B. L. Browne (2006), Bulk chemical trends at arc volcanoes are not liquid lines of descent, *Lithos*, *87*, 135–154.

Ewart, A., and W. L. Griffin (1994), Application of proton-microprobe data to trace-element partitioning in volcanic rocks, *Chem. Geol.*, *117*, 251–284.

Gamble, J. A., I. E. M. Smith, I. J. Graham, B. P. Kokelaar, J. W. Cole, B. F. Houghton, and C. J. N. Wilson (1990), The petrology, phase relations and tectonic setting of basalts from the Taupo Volcanic Zone, New Zealand and the Kermadec Island Arc-Havre Trough, SW Pacific, *J. Volcanol. Geotherm. Res.*, *43*, 253–270.

Garrison, J. M., M. K. Reagan, and K. W. W. Sims (2012), Dacite formation at Ilopango Caldera, El Salvador: U-series disequilibrium and implications for petrogenetic processes and magma storage time, *Geochem. Geophys. Geosyst.*, *13*, Q06018, doi:10.1029/2012GC004107.

Geschwind, C. H., and M. J. Rutherford (1995), Crystallization of microlites during magma ascent: The fluid mechanics of 1980–1986 eruptions at Mount St Helens, *Bull. Volcanol.*, *57*, 356–370.

Ghiorso, M. S., and B. W. Evans (2008), Themodynamics of rhombohedral oxide solid solutions and a revision of the Fe-Ti two-oxide geothermobarometer and oxygen-barometer, *Am. J. Sci.*, *308*, 957–1039.

Giordano, D., J. K. Russell, and D. B. Dingwell (2008), Viscosity of magmatic liquids: A model, *Earth Planet. Sci. Lett.*, *271*, 123–134.

Graham, I. J., and T. J. Worthington (1988), Petrogenesis of Tauhara Dacite (Taupo Volcanic Zone, New Zealand)—Evidence for magma mixing between high-alumina andesite and rhyolite, *J. Volcanol. Geotherm. Res.*, *35*, 279–294.

Graham, I. J., J. W. Cole, R. M. Briggs, J. A. Gamble, and I. E. M. Smith (1995), Petrology and petrogenesis of volcanic rocks from the Taupo Volcanic Zone: A review, *J. Volcanol. Geotherm. Res.*, *68*, 59–87.

Gravley, D. M., C. J. N. Wilson, G. S. Leonard, and J. W. Cole (2007), Double trouble: Paired ignimbrite eruptions and col-

lateral subsidence in the Taupo Volcanic Zone, New Zealand, *Geol. Soc. Bull. Am.*, *119*, 18–30.

Green, T. H., and N. J. Pearson (1985), Experimental determination of REE partition coefficients between amphibole and basaltic to andesitic liquids at high pressure, *Geochim. Cosmochim. Acta*, *49*, 1465–1468.

Harrison, A. J., and R. S. White (2004), Crustal structure of the Taupo Volcanic Zone, New Zealand: Stretching and igneous intrusion, *Geophys. Res. Lett.*, *31*, L13615, doi: 10.1029/2004GL019885.

Healy, J. (1962), Structure and volcanism in the Taupo Volcanic Zone, New Zealand, in *The Crust of the Pacific Basin, Geophys. Monogr. Ser.*, vol. *6*, edited by G. A. MacDonald and H. Kuno, pp. 151–157, AGU, Washington, D. C.

Hirose, K. (1997), Melting experiments on lherzolite KLB-1 under hydrous conditions and generation of high-magnesian andesitic melts, *Geology*, *25*, 42–44.

Kent, A. J. R., C. Darr, A. M. Koleszar, M. J. Salisbury, and K. M. Cooper (2010), Preferential eruption of andesitic magmas through recharge filtering, *Nat. Geosci.*, *3*, 631–636.

Martin, V. M., D. J. Morgan, D. A. Jerram, M. J. Caddick, D. J. Prior, and J. P. Davidson (2008), Bang! Month-scale eruption triggering at Santorini volcano, *Science*, *321*, 1178.

Mashima, H. (2004), Time scale of magma mixing between basalt and dacite estimated for the Saga-Futagoyama volcanic rocks in northwest Kyushu, southwest Japan, *J. Volcanol. Geotherm. Res.*, *131*, 333–349.

Matthews, N. E., D. M. Pyle, V. C. Smith, C. J. N. Wilson, C. Huber, and V. van Hinsberg (2012a), Quartz zoning and the pre-eruptive evolution of the ∼340 ka Whakamaru magma systems, New Zealand, *Contrib. Mineral. Petrol.*, *163*, 87–107.

Matthews, N. E., C. Huber, D. M. Pyle, and V. C. Smith (2012b), Timescales of magma recharge and reactivation of large silicic systems from Ti diffusion in quartz, *J. Petrol.*, *53*, 1385–1416.

McCanta, M. C., M. J. Rutherford, and J. E. Hammer (2007), Pre-eruptive and syn-eruptive conditions in the Black Butte, California dacite: Insight into crystallization kinetics in a silicic magma system, *J. Volcanol. Geotherm. Res.*, *160*, 263–284.

McCulloch, M. T., T. K. Kyser, J. D. Woodhead, and L. Kinsley (1994), Pb-Sr-Nd-O isotopic constraints on the origin of rhyolites from the Taupo Volcanic Zone of New Zealand: Evidence for assimilation followed by fractionation from basalt, *Contrib. Mineral. Petrol.*, *115*, 303–312.

Morgan, D. J., S. Blake, N. W. Rogers, B. De Vivo, G. Rolandi, R. Macdonald, and C. J. Hawkesworth (2004), Time scales of crystal residence and magma chamber volume from modelling of diffusion profiles in phenocrysts: Vesuvius 1944, *Earth Planet. Sci. Lett.*, *222*, 933–946.

Nagasawa, H., and C. C. Schnetzler (1971), Partitioning of rare earth, alkali, and alkaline earth elements between phenocrysts and acidic igneous magmas, *Geochim. Cosmochim. Acta*, *35*, 953–968.

Nakamura, M. (1995), Continuous mixing of crystal mush and replenished magma in the ongoing Unzen eruption, *Geology*, *23*, 807–810.

Parson, L. M., and I. C. Wright (1996), The Lau–Havre–Taupo back–arc basin: A southward propagating, multi-stage evolution from rifting to spreading, *Tectonophysics*, *263*, 1–22.

Pichavant, M., B. O. Mysen, and R. Macdonald (2002a), Source and H$_2$O content of high-MgO magmas in island arc settings: An experimental study of a primitive calc-alkaline

basalt from St. Vincent, Lesser Antilles arc, *Geochim. Cosmochim. Acta*, *66*, 2193–2209.

Putirka, K. D. (2008), Thermometers and barometers for volcanic systems, in *Minerals, Inclusions and Volcanic Processes, Rev. Mineral. Geochem.*, vol. *69*, edited by K. D. Putirka and F. J. Tepley III, pp. 61–120, Mineral. Soc. of Am., Washington, D. C.

Reubi, O., and J. Blundy (2009), A dearth of intermediate melts at subduction zone volcanoes and the petrogenesis of arc andesites, *Nature*, *461*, 1269–1274.

Ridolfi, F., and A. Renzulli (2012), Calcic amphiboles in calc-alkaline and alkaline magmas: Thermobarometric and chemometric empirical equations valid up to 1,130°C and 2.2 GPa, *Contrib. Mineral. Petrol.*, *163*, 877–895.

Ridolfi, F., A. Renzulli, and M. Puerini (2010), Stability and chemical equilibrium of amphibole in calc-alkaline magmas: An overview, new thermobarometric formulations and application to subduction-related volcanoes, *Contrib. Mineral. Petrol.*, *160*, 45–66.

Rudnick, R. L. (1995), Making continental crust, *Nature*, *378*, 571–578.

Rudnick, R. L., and D. M. Fountain (1995), Nature and composition of the continental crust: A lower crustal perspective, *Rev. Geophys.*, *33*, 267–309.

Ruprecht, P., and K. M. Cooper (2012), Integrating the uranium-series and elemental diffusion geochronometers in mixed magmas from Volcán Quizapu, Central Chile, *J. Petrol.*, *53*, 841–871.

Rutherford, M. J. (2008), Magma ascent rates, *Rev. Mineral. Petrol.*, *69*, 241–271.

Rutherford, M. J., and J. D. Devine (2002), Magmatic conditions and magma ascent as indicated by hornblende phase equilibria and reactions in the 1995–2002 Soufrière Hills magma, *J. Petrol.*, *44*, 1433–1454.

Rutherford, M. J., and P. M. Hill (1993), Magma ascent rates from amphibole breakdown: An experimental study applied to the 1980–1986 Mount St. Helens eruptions, *J. Geophys. Res.*, *93*, 11,949–11,959.

Saunders, K. E., D. J. Morgan, J. A. Baker, and R. J. Wysoczanski (2010), The magmatic evolution of the Whakamaru Supereruption, New Zealand, constrained by a microanalytical study of plagioclase and quartz, *J. Petrol.*, *51*, 2465–2488.

Scaillet, B., F. Holtz, and M. Pichavant (1998), Phase equilibrium constraints on the viscosity of silicic magmas 1. Volcanic-plutonic comparison, *J. Geophys. Res.*, *103*, 27,257–27,266.

Schiano, P., M. Monzier, J.-P. Eissen, H. Martin, and K. T. Koga (2010), Simple mixing as the major control of the evolution of volcanic suites in the Ecuadorian Andes, *Contrib. Mineral. Petrol.*, *160*, 297–312.

Severs, M. J., J. S. Beard, L. Fedele, J. M. Hanchar, S. R. Mutchler, and R. J. Bodnar (2009), Partitioning behaviour of trace elements between dacitic melt and plagioclase, orthopyroxene, and clinopyroxene based on laser ablation ICPMS analysis of silicate melt inclusions, *Geochim. Cosmochim. Acta*, *73*, 2123–2141.

Sisson, T. W. (1994), Hornblende-melt trace element partitioning measured by ion microprobe, *Chem. Geol.*, *117*, 331–344.

Sobolev, A. V., A. A. Migidosov, and M. V. Portnyagin (1996), Incompatible element partitioning between clinopyroxene and basalt liquid revealed by the study of melt inclusions in minerals from Troodos Lavas, Cyprus, *Petrologiya*, *4*, 307–317.

Sparks, R. S. J., and L. A. Marshall (1986), Thermal and mechanical constraints on mixing between mafic and silicic magmas, *J. Volcanol. Geotherm. Res.*, *29*, 99–124.

Stern, T., W. Stratford, A. Seward, M. Henderson, M. Savage, E. Smith, A. Benson, S. Greve, and M. Salmon (2010), Crust-mantle structure of the central North Island, New Zealand, based on seismological observations, *J. Volcanol. Geotherm. Res.*, *190*, 58–74.

Sutton, A. N., S. Blake, and C. J. N. Wilson (1995), An outline geochemistry of rhyolite eruptives from Taupo volcanic centre, New Zealand, *J. Volcanol. Geotherm. Res.*, *68*, 153–175.

Tieopolo, M., R. Oberti, A. Zanetti, R. Vannucci, and S. F. Foley (2007), Trace element partitioning between amphibole and silicate melt, *Rev. Mineral. Geochem.*, *67*, 417–452.

Turner, S. P., B. Bourdon, C. J. Hawkesworth, and P. Evans (2000), ^{226}Ra-^{230}Th evidence for multiple dehydration events, rapid melt ascent and the time scales of differentiation beneath the Tonga-Kermadec island arc, *Earth Planet. Sci. Lett.*, *179*, 581–593.

Venezky, D. Y., and M. J. Rutherford (1999), Petrology and Fe-Ti oxide re-equilibration of the 1991 Mount Unzen mixed magma, *J. Volcanol. Geotherm. Res.*, *89*, 213–230.

Wilson, C. J. N. (1993), Stratigraphy, chronology, styles and dynamics of late Quaternary eruptions from Taupo volcano, New Zealand, *Philos. Trans. R. Soc. London A*, *343*, 205–306.

Wilson, C. J. N., B. F. Houghton, M. O. McWilliams, M. A. Lanphere, S. D. Weaver, and R. M. Briggs (1995), Volcanic and structural evolution of Taupo Volcanic Zone, New Zealand: A review, *J. Volcanol. Geotherm. Res.*, *68*, 1–28.

Worthington, T. J. (1985), Geology and petrology of the Tauhara Volcanic Complex, Taupo, New Zealand, MSc thesis, Victoria Univ. of Wellington, New Zealand.

Zajacz, Z., and W. Halter (2007), LA-ICPMS analyses of silicate melt inclusions in co-precipitated minerals: Quantification, data analysis and mineral/melt partitioning, *Geochim. Cosmochim. Acta*, *71*, 1021–1040.